Aus der Klinik und Poliklinik für Nuklearmedizin Klinikum
der Ludwig-Maximilians-Universität München
Vorstand: Prof. Dr. Peter Bartenstein

In vivo Untersuchungen zerebraler β-Amyloidose und Neuroinflammation mittels Positronen-Emissions-Tomographie in einem Amyloid Mausmodell ohne APP Überexpression

Dissertation
zum Erwerb des Doktorgrades der Medizin an
der Medizinischen Fakultät der
Ludwig-Maximilians-Universität zu München

vorgelegt von

Christian Alexander Sacher
aus
Kumhausen

2022

Mit Genehmigung der Medizinischen Fakultät
der Universität München

Berichterstatter:	Priv.-Doz. Dr. med. Matthias Brendel
Mitberichterstatter:	Prof. Dr. Oliver Pogarell Prof. Dr. Johannes Levin Prof. Dr. Harald Steiner
Mitbetreuung durch den promovierten Mitarbeiter:	Dr. Leonie Beyer
Dekan:	Prof. Dr. med. Thomas Gudermann
Tag der mündlichen Prüfung:	17.02.2022

I. Eidesstattliche Versicherung

Sacher, Christian Alexander

Name, Vorname

Ich erkläre hiermit an Eides statt, dass ich die vorliegende Dissertation mit dem Titel

In vivo Untersuchungen zerebraler β-Amyloidose und Neuroinflammation mittels Positronen-Emissions-Tomographie in einem Amyloid Mausmodell ohne APP Überexpression

selbständig verfasst, mich außer der angegebenen keiner weiteren Hilfsmittel bedient und alle Erkenntnisse, die aus dem Schrifttum ganz oder annähernd übernommen sind, als solche kenntlich gemacht und nach ihrer Herkunft unter Bezeichnung der Fundstelle einzeln nachgewiesen habe.

Ich erkläre des Weiteren, dass die hier vorgelegte Dissertation nicht in gleicher oder in ähnlicher Form bei einer anderen Stelle zur Erlangung eines akademischen Grades eingereicht wurde.

Landshut, 17.02.2022 — Ort, Datum

Christian Sacher — Unterschrift Doktorandin bzw. Doktorand

Kumulative Dissertation gemäß § 4a der Promotionsordnung

II. Inhaltsverzeichnis

III. Abkürzungsverzeichnis

APP	Amyloid Vorläuferprotein
Aβ	Amyloid Beta Peptid, β-Amyloid
AI	Asymmetrie-Index
^{11}C	Kohlenstoff-Isotop mit der Massenzahl 11
CTX	Frontaler Cortex
FAD	Familiäre Alzheimer Krankheit
^{18}F	Fluor-Isotop mit der Massenzahl 18
HIP	Hippocampus
KI	Konfidenzintervall
mo	Monate
MWM	Morris-Wasserlabyrinth
PET	Positronen-Emissions-Tomographie
PAG	Periaquäduktales Grau
SUV	Standard-Aufnahmewert
SUVR	relativer Standard-Aufnahmewert
Trem2	Triggering receptor expressed on myeloid cells 2
TSPO	18-kDa-Translokator-Protein
WT	Wildtyp
µPET	Kleintier PET

IV. Publikationen der kumulativen Dissertation

Die vorliegende kumulative Dissertation umfasst zwei bereits publizierte Manuskripte:

Sacher, C.; Blume, T.; Beyer, L.; Peters F.; Eckenweber, F.; Sgobio, C.; Deussing, M.; Albert, N.L.; Unterrainer, M.; Lindner, S.; Gildehaus F.; von Ungern-Sternberg, B.; Brzak, I.; Neumann, U.; Saito, T.; Saido, T.C.; Bartenstein, P.; Rominger, A.; Herms, J.; Brendel, M.; **Longitudinal PET Monitoring of Amyloidosis and Microglial Activation in a Second-Generation Amyloid-β Mouse Model.** J Nucl Med. 2019 60(12):1787-179

Sacher, C.; Blume, T.; Beyer, L.; Biechele, G.; Sauerbeck, J.; Eckenweber, F.; Deussing, M.; Focke, C.; Parhizkar, S.; Lindner, S.; Gildehaus F.; von Ungern-Sternberg B.; Baumann, K.; Tahirovic, S.; Kleinberger, G.; Willem, M.; Haass, C.; Bartenstein, P.; Cumming, P.; Rominger, A.; Herms, J.; Brendel, M.; **Asymmetry of Fibrillar Plaque Burden in Amyloid Mouse Models.** J Nucl Med. 2020 61(12):1825-1831

Beschreibung des Eigenanteiles an der Publikation „**Longitudinal PET Monitoring of Amyloidosis and Microglial Activation in a Second-Generation Amyloid-β Mouse Model**“:

Konzeption des Studiendesigns gemeinsam mit dem AG-Leiter. Selbständige Durchführung aller PET-Experimente sowie anschließende Analyse und statistische Auswertung der erhobenen PET-Daten. Selbständige statistische Auswertung der erhobenen histochemischen und biochemischen Daten sowie der erhobenen Daten der Verhaltensversuche. Abschließend selbständige Interpretation aller ausgewerteten Daten sowie Verfassung des ersten Manuskript-Drafts. Mitbeteiligung bei der Überwachung der Pflege und Gesundheit der Versuchstiere.

Beschreibung des Eigenanteiles an der Publikation **„Asymmetry of Fibrillar Plaque Burden in Amyloid Mouse Models**“:

Selbständige primäre Konzeption des Studiendesigns unter Supervision des AG-Leiters. Selbständige Recherche aller erhobenen Rohdaten der PET Scans aus vorherigen internen Studien mit anschließend selbständiger standardisierter Analyse und statistischer Auswertung. Abschließend selbständige Interpretation der ausgewerteten PET-Daten sowie Verfassung des ersten Manuskript-Drafts.

1. Einführung

Im Jahr 2015 waren weltweit etwa 47 Millionen Menschen an einer Demenz erkrankt, wobei 50-70% auf die Alzheimer Erkrankung entfielen (Winblad, Amouyel et al. 2016). Den Hauptrisikofaktor an Alzheimer zu erkranken stellt das steigende Lebensalter dar (Querfurth and LaFerla 2010). In diesem Zusammenhang wird es vor allem in Industrienationen aufgrund des demographischen Wandels zukünftig zu einer enormen sozioökonomischen Belastung der Gesundheitssysteme kommen (Ziegler-Graham, Brookmeyer et al. 2008). Angesichts dieser ernstzunehmenden epidemiologischen Prognose werden präventive Arzneimittel dringend benötigt. Bisher konnten aber lediglich symptomatische Therapeutika in Form von Acetylcholinesterasehemmern und NMDA-Antagonisten etabliert werden, welche die Progression der Erkrankung nur geringfügig verzögern (Schneider 2013). Hinsichtlich krankheitsmodifizierender Medikamente konnte die Pharmaindustrie jedoch trotz einer hohen Anzahl vielversprechender Arzneimittelkandidaten bisher keine Arzneimittelzulassungen erreichen (Pardridge 2020). Zuletzt befand sich der gegen Amyloid Beta Peptid (β-Amyloid) gerichtete monoklonale Antikörper Aducanumab in den USA kurz vor einer möglichen Zulassung. Jedoch konnte nur in einer von zwei groß angelegten klinischen Studien eine grenzwertig signifikante Verbesserung im Vergleich zu Placebo gezeigt werden (Sabbagh and Cummings 2020). Die Diskrepanzen in den Ergebnissen zwischen den beiden Studien wurden von externen Beratern der US Arzneimittelbehörde „Food and Drug Administration“ (FDA) letztlich als zu groß eingestuft, um eine Wirksamkeit von Aducanumab zu belegen (Combined FDA and applicant PCNS Drugs Advisory Committee Briefing document. https://www.fda.gov/media/143502/download. November 6, 2020). Den Misserfolgen der Pharmaindustrie hinsichtlich der Zulassung krankheitsmodifizierender

Medikamente können viele Ursachen zu Grunde liegen. Hierzu zählen beispielsweise falsch gewählte Zeitpunkte therapeutischer Interventionen. Studien an Inhibitoren des Enzyms Beta-Sekretase 1 (BACE1) wie Verubecestat zeigten auf, dass bereits bei Auftreten leichter kognitiver Symptome kein krankheitsmodifizierender Effekt mehr erzielt werden kann (Egan, Kost et al. 2018). Weitere Probleme ergeben sich durch den Mangel an präzisen Biomarkern zur Evaluation präklinischer und klinischer Medikamentenstudien. Dies wurde in Phase-III-Studien zum anti-β-Amyloid Antikörper Bapineuzumab ersichtlich, wobei weder die in-vitro Quantifizierung der Liquorkonzentration von phosphoryliertem Tau-Protein, noch die in-vivo Quantifizierung von β-Amyloid mittels [^{11}C]-Pittsburgh Compound B (PiB) Amyloid-Positronen-Emissions-Tomographie (PET) als verlässlicher Screening-Parameter geeignet war (Salloway, Sperling et al. 2014).

Um geeignete Biomarker und letztlich potentiell krankheitsmodifizierende Medikamente zu erproben, spielen präklinische Studien unter dem Einsatz geeigneter Alzheimer Mausmodelle eine entscheidende Rolle (Sasaguri, Nilsson et al. 2017).

1.1 Pathophysiologie der Amyloidakkumulation und der Neuroinflammation im Rahmen der Alzheimer Krankheit

Klinisch ist die Alzheimer Erkrankung durch frühe Gedächtnisdefizite gekennzeichnet, gefolgt von einem Rückgang weiterer kognitiver Funktionen (Dubois, Padovani et al. 2016). Die Neuropathologie beginnt sich jedoch bereits bis zu 20 Jahre vor dem Einsetzen der ersten Symptome zu manifestieren (Bateman, Xiong et al. 2012). Diese umfasst die Akkumulation von β-Amyloid (Aβ) zu extrazellulären β-Amyloid-Plaques, hyperphosphoryliertem Tau-Protein zu intrazellulären Neurofibrillen-Bündeln sowie die Aktivierung mehrerer neuroinflammatorischer Signalkaskaden, gefolgt von dem Verlust

neuronaler Zellen hauptsächlich in der Großhirnrinde und im Hippocampus (Braak and Braak 1991, Querfurth and LaFerla 2010). β-Amyloid entsteht aus der Proteolyse des Amyloid-Vorläuferproteins (engl.: Amyloid Precursor Protein, APP) durch die aufeinanderfolgenden enzymatischen Spaltungen mittels β-Sekretase und γ-Sekretase (Querfurth and LaFerla 2010). Die beiden wichtigsten Isoformen sind einerseits das zur Aggregation neigende Aβ42 sowie andererseits Aβ40, bei welchem ein neuroprotektiver Effekt vermutet wird (Kim, Onstead et al. 2007, Nilsson, Saito et al. 2014). Ein Ungleichgewicht zwischen Produktion und Abbau führt zu einer Akkumulation von β-Amyloid, welches spontan zu Fibrillen aggregieren kann. Diese Fibrillen wiederum bilden die unlöslichen faserartigen Anteile der fortgeschrittenen, kompakten Plaques. β-Amyloid kann jedoch auch zu löslichen Oligomeren aggregieren, die wiederum zu frühen, intermediären β-Amyloid-Aggregaten verschmelzen. Lösliche Oligomere und intermediäre β-Amyloid-Aggregate gelten als die neurotoxischsten Formen von β-Amyloid (Querfurth and LaFerla 2010). Im Gehirn befinden sich phagozytierende Zellen, sogenannte Mikroglia, welche Infektionen, beschädigte Zellen oder toxisches Material wie beispielsweise β-Amyloid erkennen und aus dem Gehirn entfernen können. Aktivierte Mikroglia exprimieren bestimmte Zelloberflächenrezeptoren, um den Abbau und die Phagozytose von β-Amyloid zu fördern. Beispielsweise agiert der „Triggering receptor expressed on myeloid cells 2“ (Trem2) als Mediator und Biomarker des phagozytischen Abbaus von β-Amyloid (Heneka, Carson et al. 2015). Mutationen in mikroglialen Alzheimer Risikogenen wie Trem2 oder Apolipoprotein E (APOE) spielen eine entscheidende Rolle bei der Pathogenese der Alzheimer Erkrankung, da sie die Aggregation von β-Amyloid und somit die Fibrillarität und Toxizität der β-Amyloid-Plaques beeinflussen (Cuyvers and Sleegers 2016, Parhizkar, Arzberger et al. 2019). In einer kürzlich erschienen

präklinischen Studie konnte zudem gezeigt werden, dass insbesondere dichte, fibrilläre Plaques zu einer verstärkten Migration von krankheitsspezifischer Mikroglia führen, welche eine reduzierte phagozytäre Funktion aufweisen und zudem eine Vielzahl neurotoxischer Proteine exprimieren (Sebastian Monasor, Muller et al. 2020).

1.2 Bildgebung der Amyloidakkumulation und der Neuroinflammation

Im Jahr 2018 wurden von der Arbeitsgruppe des National Institute on Aging (NIA) und der Alzheimer's Association (AA) neue Kriterien zur Diagnostik der Alzheimer Erkrankung publiziert. Dabei sind nicht mehr klinische Symptome wie Orientierungslosigkeit oder Gedächtnisverlust im Verbund mit neuropsychologischen Testbatterien diagnostisch entscheidend, sondern zunehmend die Biomarker-Information von Relevanz. Wegweisend ist dabei die immunchemische Quantifizierung von β-Amyloid und phosphoryliertem Tau-Protein im Liquor cerebrospinalis (engl.: Cerebrospinal fluid, CSF) oder im Blutplasma. Zu weiteren CSF- und Plasmabiomarkern zählen Neurogranin zum Nachweis synaptischer Dysfunktion, Neurofilament light chain (NFL) zum Nachweis der Neurodegeneration sowie YKL-40 zur Detektion neuroinflammatorischer Prozesse. Neben invasiven Biomarkern spielen auch bildgebende Verfahren eine entscheidende Rolle. Einerseits können Zeichen der Neurodegeneration mittels struktureller Magnetresonanztomographie (MRT) oder in der Fluorodeoxyglucose (FDG)-PET erfasst werden. Zusätzlich ist es möglich, krankheitstypische Ablagerungen in Form von parenchymalen Neurofibrillen und β-Amyloid mittels PET zu detektieren.(Jack, Bennett et al. 2018, Palmqvist, Insel et al. 2019).

In der Hoffnung präventive Medikamente zu entwickeln, hat sich im Laufe der letzten Jahrzehnte der Schwerpunkt der Alzheimer-Forschung auf die Charakterisierung der

frühen Stadien der Erkrankung fokussiert (Sepulcre, Sabuncu et al. 2013). Insbesondere die in vivo Quantifizierung von β-Amyloid mit Hilfe molekularer Bildgebung mittels PET könnte eine entscheidende Rolle bei der Entwicklung krankheitsmodulierender Medikamente spielen, initial zur frühzeitigen Diagnosesicherung und sekundär zur Evaluation eines Therapieansprechens. Der erste zugelassene Amyloid-Radiotracer [^{11}C]-Pittsburgh Compound B (PiB) bindet selektiv an fibrillärem β-Amyloid, hat jedoch nur eine relativ kurze Halbwertszeit von 20 min. Dadurch beschränkt sich sein Einsatz auf Zentren mit unmittelbarer Anbindung an ein Zyklotron (Fodero-Tavoletti, Brockschnieder et al. 2012). Folglich wurden die [^{18}F]-markierten Substanzen [^{18}F]-florbetapir, [^{18}F]-flutemetamol und [^{18}F]-florbetaben mit einer längeren Halbwertszeit von 110 min erfolgreich in der klinischen Diagnostik etabliert (Vandenberghe, Van Laere et al. 2010, Clark, Schneider et al. 2011). Für [^{18}F]-florbetaben wird ebenfalls eine verstärkte Bindungsaffinität an fibrillärem β-Amyloid beschrieben (Barthel and Sabri 2011).

Des Weiteren ermöglicht die PET die in vivo Detektion neuroinflammatorischer Prozesse, die damit eine Schlüsselrolle bei der Testung potenziell anti-inflammatorischer Interventionen einnimmt. Dafür verwendet man Radiotracer, die an das 18-kD-Translokator-Protein (TSPO) binden. Dieses Membranprotein wird an der äußeren Mitochondrienwand aktivierter Mikroglia hoch exprimiert und dient somit als weiterer Biomarker der Neuroinflammation (Heneka, Carson et al. 2015). Primär wurden zunächst ebenfalls [^{11}C] markierte Substanzen zur molekularen Bildgebung der Neuroinflammation im Rahmen von Patientenstudien eingesetzt. Häufig verwendet wurde dabei der Radiotracer [^{11}C]-PK11195, dessen erhöhte Aufnahme in das Gehirn bei Alzheimer Patienten erstmals 2001 durch Cagnin und Koautoren beschrieben wurde (Cagnin, Brooks et al. 2001). Dieser Tracer wies jedoch einige Nachteile auf, wie

etwa eine geringe Bindungsaffinität sowie eine niedrige Bindungsspezifität für TSPO, die wiederum zu einem geringen Signal-Rausch-Verhältnis führten. Darüber hinaus ergaben sich die oben beschriebenen logistischen Schwierigkeiten aufgrund der kurzen Halbwertszeit von [^{11}C] (Edison, Donat et al. 2018). In Folge dessen wurde eine Reihe neuerer TSPO-Liganden entwickelt. Der Radiotracer [^{18}F]-GE-180 lieferte dabei die vielversprechendsten Ergebnisse hinsichtlich der Aufnahme in das Gehirn sowie hinsichtlich Bindungsaffinität und Bindungsspezifität (Zanotti-Fregonara, Pascual et al. 2018).

1.3 Kleintier PET

Die Bildgebung mittels Kleintier PET stellt eine optimale Schnittstelle zwischen Tiermodell und humaner Forschung dar. Aufgrund vergleichbarer radiopharmazeutischer Eigenschaften hinsichtlich Hirnpermeabilität und Bindungsaffinität eröffnet sich die Möglichkeit der translationalen Bildgebung humanpathologischer Phänotypen in genetisch veränderten Tiermodellen (Zimmer, Parent et al. 2014). In Bezug auf die Alzheimer Erkrankung ermöglicht die Anwendung von Amyloid- und TSPO-Tracern die Durchführung präklinischer Längsschnittstudien in Mausmodellen zur in vivo Verlaufsbeurteilung möglicher Arzneimittelinterventionen. Die Anwendung der PET im Kleintierbereich wird durch speziell konfigurierte PET-Scanner realisiert. Bereits in den späten 1990er Jahren wurden die ersten Prototypen entsprechender PET Systeme getestet. Dabei zeigten sich signifikante Vorteile hinsichtlich räumlicher Auflösung, Sensitivität und Bildqualität. Seit 2000 etablierte sich eine Vielzahl unterschiedlicher kommerziell nutzbarer Kleintier PET-Scanner, deren räumliche Auflösung sowie Sensitivität sich kontinuierlich verbessern (Goertzen, Bao et al. 2012). Zusätzlich ermöglichen spezielle aus Plexiglas konfigurierte Mehrfach-

Maushalterungen ein verbessertes ökonomisches Arbeiten, wobei bis zu acht Mäuse gleichzeitig gemessen werden können (Rominger, Mille et al. 2010). Zur Auswertung der PET Daten erfolgt in präklinischen Studien eine relative Quantifizierung mittels Bestimmung des relativen Standard-Aufnahmewertes (engl.: Standardized-Uptake-Value-Ratio, SUVR). Dieser berechnet sich anhand der Division eines bestimmten Zielvolumens durch ein möglichst pathologiefreies Referenzvolumen. Als zerebrale Vergleichsregionen ohne spezifische Tracer-Bindung dienten bisher beispielsweise die weiße Substanz oder das Cerebellum (Brendel, Probst et al. 2016).

1.4 Mausmodelle der Alzheimer Krankheit

Alzheimer Mausmodelle gelten als wichtige Mittel zur Erforschung der zugrunde liegenden molekularen Mechanismen der Erkrankung sowie der Testung potenzieller Therapeutika in präklinischen Studien (Webster, Bachstetter et al. 2014, Puzzo, Gulisano et al. 2015). Die Identifikation familiärer Alzheimer (engl.: Familial Alzheimer Disease, FAD) Mutationen im APP-Gen bildete die Grundlage für die Entwicklung einer Vielzahl transgener Amyloid Mausmodelle (Hardy and Allsop 1991, Hsiao 1998). Dadurch, dass die genetisch veränderte APP-Sequenz an einer zufälligen Stelle ins Empfänger-Genom integriert wird („random-integration“), kann diese auch in sehr transkriptionsaktiven Bereichen der DNA zu liegen kommen. Die daraus resultierende APP-Überexpression führt nach deren Spaltung durch die verschiedenen Sekretasen nicht nur zur gewünschten Überproduktion von β-Amyloid, sondern auch zu vielen weiteren Spaltprodukten. Da deren Einfluss auf die Alzheimer Erkrankung noch nicht ausreichend erforscht ist, können dabei auch verfälschte Phänotypen entstehen (Sasaguri, Nilsson et al. 2017).

Um das Problem der APP-Überexpression zu umgehen, wurden knock-in Amyloid Mausmodelle der “zweiten Generation“ entwickelt. Für das Modell APP-NL-G-F wurde zunächst die murine β-Amyloid-Sequenz mittels eines Austauschs von drei Aminosäuren (G601R, F606Y und R609H) humanisiert. Zusätzlich setzte man drei FAD-assoziierte Mutationen in den endogenen APP-Lokus ein (Saito, Matsuba et al. 2014): Eine schwedische Mutation (KM595 / 596NL), welche die gesamte β-Amyloid-Produktion erhöht (Citron, Oltersdorf et al. 1992). Eine Beyreuther / Iberische Mutation (I641F), welche das Verhältnis von Aβ42/Aβ40 erhöht sowie eine arktische Mutation (E618G), welche die Aggregation von β-Amyloid fördert (Lichtenthaler, Wang et al. 1999, Tsubuki, Takaki et al. 2003). Abschließend wurde dieses gesamte Genkonstrukt mittels knock-in gezielt in den APP-Genlokus eingefügt. Unter Kontrolle des korrekten Promotors wird APP in physiologischer Quantität exprimiert. Homozygote APP-NL-G-F Mäuse zeigen eine fortschreitende β-Amyloid-Akkumulation und eine reaktive mikrogliale Aktivierung ab einem Alter von zwei Monaten und Verhaltensveränderungen in Form einer verringerten räumlichen Lernfähigkeit im Alter von 8 bis 12 Monaten (Saito, Matsuba et al. 2014, Masuda, Kobayashi et al. 2016). Neuste Studien konnten zeigen, dass sich dabei die Morphologie der β-Amyloid-Plaques im Vergleich zu transgenen Mausmodellen unterscheidet. Statt kompakter, [^{18}F]-florbetaben-affiner, fibrillärer Plaques, bilden sich im APP-NL-G-F Modell eher lockere, baumwollartige Plaques (Sebastian Monasor, Muller et al. 2020). In wieweit diese mittels Amyloid-PET erfasste werden können, ist bisher noch nicht bekannt.

1.5 Kleintier PET Studien zur Detektion der Amyloidakkumulation und der Neuroinflammation

Sowohl in Bezug auf die Amyloid-Pathologie als auch auf die Neuroinflammation konnten bisherige präklinische Kleintierstudien bereits überzeugende quantitative

Ergebnisse durch die PET Bildgebung liefern. Während zu knock-in Amyloid Mausmodellen bislang noch keine Ergebnisse vorlagen, konnten diverse transgene Mausmodelle schon erfolgreich mittels [^{18}F]-florbetaben Amyloid- und [^{18}F]-GE-180 TSPO-Kleintier PET untersucht werden. Hierzu zählen beispielsweise die Modelle APP/PS1, PS2APP und APP-SL70. Bei diesen durch eine Überexpression von APP-gekennzeichneten Amyloid Mausmodellen waren im Vergleich mit Kontrolltieren jeweils ein ansteigendes PET-Signal bei steigendem Lebensalter nachweisbar. Durch die duale Bildgebung konnte dabei außerdem ein signifikanter Zusammenhang zwischen β-Amyloid-Ablagerungen und aktivierter Mikroglia gezeigt werden. Darüber hinaus lieferte die Validierung durch immunhistochemische und zum Teil biochemische Analysen eine exzellente Korrelation. Standardmäßig wurden dabei die Mäuse nach dem letzten Nachverfolgungsscan euthanasiert und je eine Hirnhemisphäre für die jeweilige Analyse verwendet (Brendel, Probst et al. 2016, Blume, Focke et al. 2018, Focke, Blume et al. 2019, Parhizkar, Arzberger et al. 2019).

Ziel dieser Arbeit war es, insbesondere vor dem Hintergrund eines niedrigen Anteils an kompakten, [^{18}F]-florbetaben-affinen, fibrillären β-Amyloid-Plaques im Mausmodell APP-NL-G-F, die genannte Methodik erstmals auf ein knock-in Mausmodell zu übertragen.

1.6 Asymmetrisches Auftreten der Neuropathologie bei Alzheimer Krankheit

Bei klinischen PET-Untersuchungen am Menschen wird häufig ein asymmetrisches Auftreten der Alzheimer Neuropathologie beobachtet. Aufgrund der möglichen Auswirkung auf den Phänotyp existieren bereits einige klinische PET-Studien zu dieser Thematik (Ossenkoppele, Schonhaut et al. 2016, Tetzloff, Graff-Radford et al. 2018). Eine 2015 erschiene PET-Studie konnte zeigen, dass die asymmetrische räumliche

Verteilung von β-Amyloid-Plaques positiv mit einer ipsilateral asymmetrischen Neurodegeneration korreliert. Zusätzlich wurde dabei eine linksseitige Prädominanz der β-Amyloid-Plaques mit einer signifikant stärker ausgeprägten Sprachstörung in Zusammenhang gebracht (Frings, Hellwig et al. 2015). Obwohl es bereits auch erste Hinweise auf ein asymmetrisches Auftreten der β-Amyloid-Plaques in Amyloid Mausmodellen gibt, wurde dieses Phänomen bisher noch nicht systematisch untersucht (Rominger, Brendel et al. 2013).

In diesem Zusammenhang ergab sich als weiteres Ziel dieser Arbeit, mittels Amyloid-Kleintier PET das asymmetrische Auftreten von β-Amyloid-Plaques in bereits etablierten Amyloid Mausmodellen zu untersuchen und eine damit assoziierte Altersabhängigkeit der Versuchstiere zu eruieren. Darüber hinaus wurde überprüft, ob ein Zusammenhang zwischen asymmetrischer Amyloid-Pathologie und ipsilateraler Neuroinflammation besteht.

2. Inhalte der Promotionsarbeit

2.1 Longitudinale Evaluierung eines knock-in Mausmodelles mittels Amyloid- und TSPO-PET

Die APP-Überexpression in bereits etablierten transgenen Amyloid Mausmodellen wird im Modell APP-NL-G-F mithilfe eines Knock-ins umgangen. Aufgrund der damit verbundenen Abnahme verfälschender Phänotypen könnte sich dieses Mausmodell besonders für zukünftige präklinische Therapiestudien sehr gut eignen. Das Ziel dieser wissenschaftlichen Arbeit bestand in dem erstmaligen longitudinalen in vivo Monitoring der Amyloid-Pathologie und der Neuroinflammation im knock-in Amyloid Mausmodell APP-NL-G-F.

Hierbei wurden gemischtgeschlechtliche Gruppen von homozygoten (N = 20) und heterozygoten (N = 21) APP-NL-G-F Mäusen in einem longitudinalen Versuchsaufbau zu Studienbeginn (Alter: 2,5 Monate) sowie zu drei späteren Zeitpunkten (Alter: 5 Monate, 7,5 Monate und 10 Monate) unter Verwendung des Amyloid-Tracers [^{18}F]-florbetaben und des TSPO-Tracers [^{18}F]-GE-180 gescannt. Als Kontrollgruppe dienten Wildtyp-Mäuse, welche im Alter von 2,5 und 10 Monaten (jeweils N = 6) gescannt wurden. Nach dem finalen PET Scan durchliefen alle verfügbaren Mäuse eine kognitive Testung mit Hilfe eines Morris-Wasserlabyrinths. Nach den Verhaltenstests wurden die Tiere mittels einer tiefen Betäubung euthanasiert, anschließend transkardial perfundiert und das Gehirn für die abschließenden biochemischen und (immun)histochemischen Analysen extrahiert. Mindestens vier Hirnhemisphären pro Genotyp wurden für die jeweiligen Analysen verwendet, wobei die Auswahl der jeweiligen Hirnhemisphäre nach dem Zufallsprinzip erfolgte. Biochemisch wurden Aβ40 und Aβ42 sowie Trem2 bestimmt. Die fibrilläre β-Amyloid-Plaque-Last wurde histochemisch mit dem Fluoreszenzfarbstoff Methoxy-X04 (Tocris) nachgewiesen. Die immunhistochemische Quantifizierung der aktivierten Mikroglia erfolgte durch den Antikörper Iba1 (Wako).

Zunächst musste bei der Auswertung der Ergebnisse ein modellspezifisches Problem gelöst werden: Histochemische Analysen konnten eine ubiquitäre Plaque-Last im Gehirn der APP-NL-G-F Mäuse zeigen. Dadurch war es primär nicht möglich, die bisher etablierte weiße Substanz oder das Cerebellum als Referenzregion zur Berechnung des SUVR zu verwenden. Unter Zusammenschau mit voxelbasierten Vergleichen von SUV-Bildern zwischen APP-NL-G-F Mäusen und Wildtypen konnte schließlich das periaquäduktale Grau im Mesencephalon als geeignete pathologiefreie Pseudoreferenzregion bestimmt werden **(Abb. 1)**.

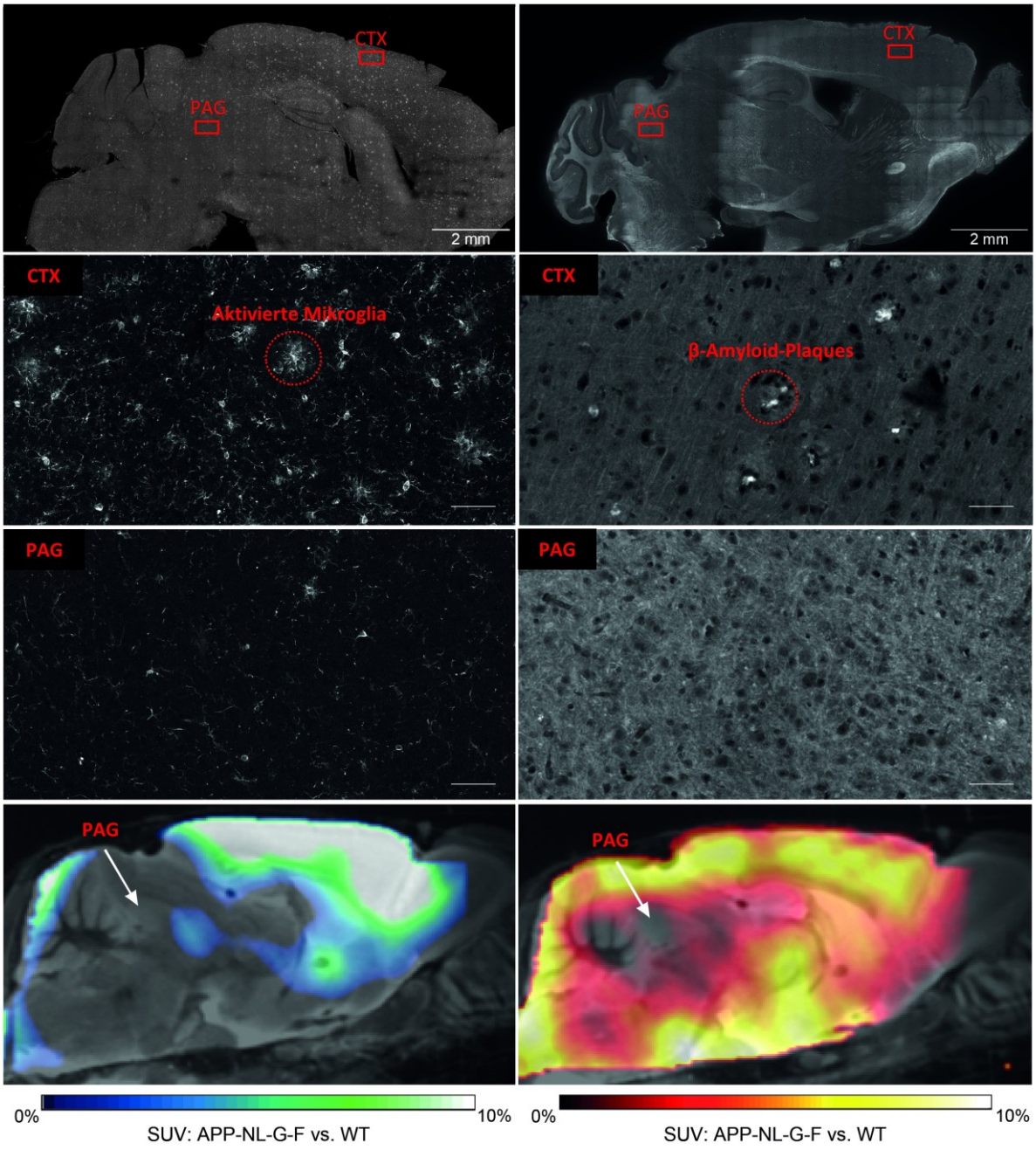

Abbildung 1: (Immun)histochemische Analysen von 10 Monate alten APP-NL-G-F Mäusen zeigten im Bereich des periaquäduktalen Graus (PAG) eine geringere mikrogliale Aktivierung (links, Iba-1) sowie weniger Aβ-Ablagerungen (rechts, Methoxy-X04) im Vergleich zum Cortex (CTX). Die Eignung des PAG (weiße Pfeile) als Pseudoreferenzregion wurde mit voxelbasierten Vergleichen des SUV von TSPO- (unterste Reihe, links) und Aβ-PET Bildern (unterste Reihe, rechts) zwischen APP-NL-G-F Mäusen und Wildtypen (WT) bestätigt.

Als Zielvolumina wurden der frontale Cortex (CTX) und der Hippocampus (HIP) gewählt, welche zur Berechnung des SUVR ins Verhältnis zu dem als Referenzvolumen dienende PAG gesetzt wurden ($SUVR_{CTX/PAG}$; $SUVR_{HIP/PAG}$) **(Abb. 2).**

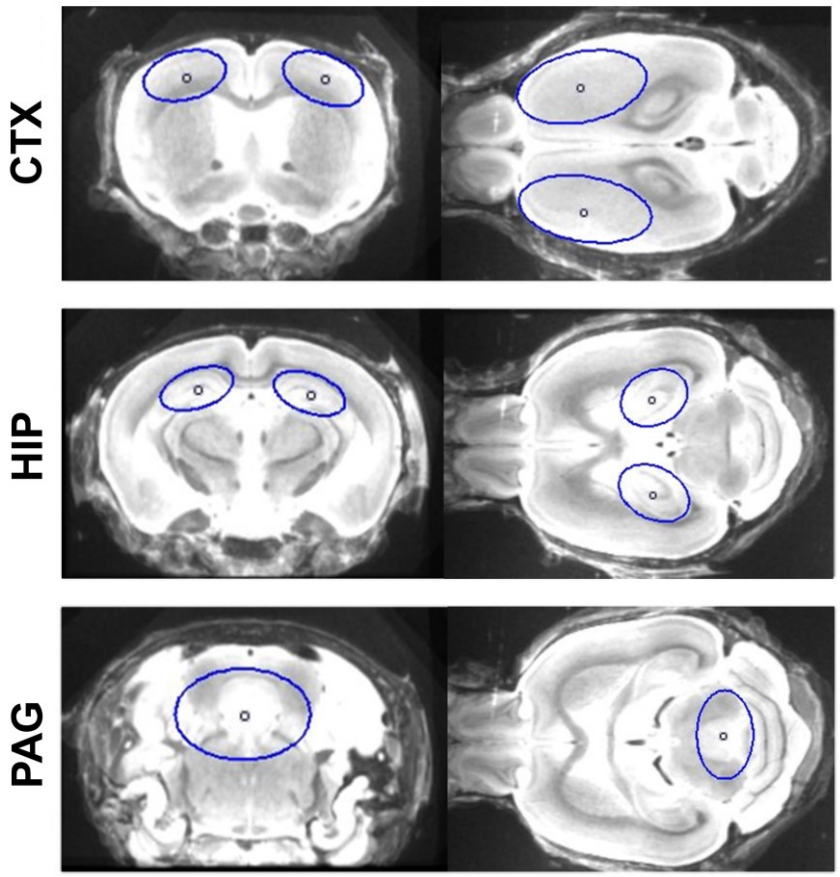

Abbildung 2: Definitionen von kortikalen (CTX) und hippocampalen (HIP) Zielvolumina sowie des periaquäduktalen Graus (PAG) als Referenzvolumen im MRT-Atlas des Mausgehirnes in coronalen und axialen Schnitten.

Homozygote APP-NL-G-F Mäuse zeigten zwischen dem ersten (Alter: 2,5 Monate) und letzten Nachverfolgungsscan (Alter: 10 Monate) einen signifikanten Anstieg des SUVR im Bereich des frontalen Cortex sowie des Hippocampus sowohl im Amyloid-PET ($SUVR_{CTX/PAG}$ +9,1%; $SUVR_{HIP/PAG}$ +3,8%; **Abb. 3 A, C**) als auch im TSPO-PET

(SUVR$_{CTX/PAG}$ +19,8%; SUVR$_{HIP/PAG}$ +14,2%; **Abb. 3 B, D**). Heterozygote APP-NL-G-F Mäuse zeigten wiederum keinen signifikanten SUVR-Anstieg mit zunehmendem Alter.

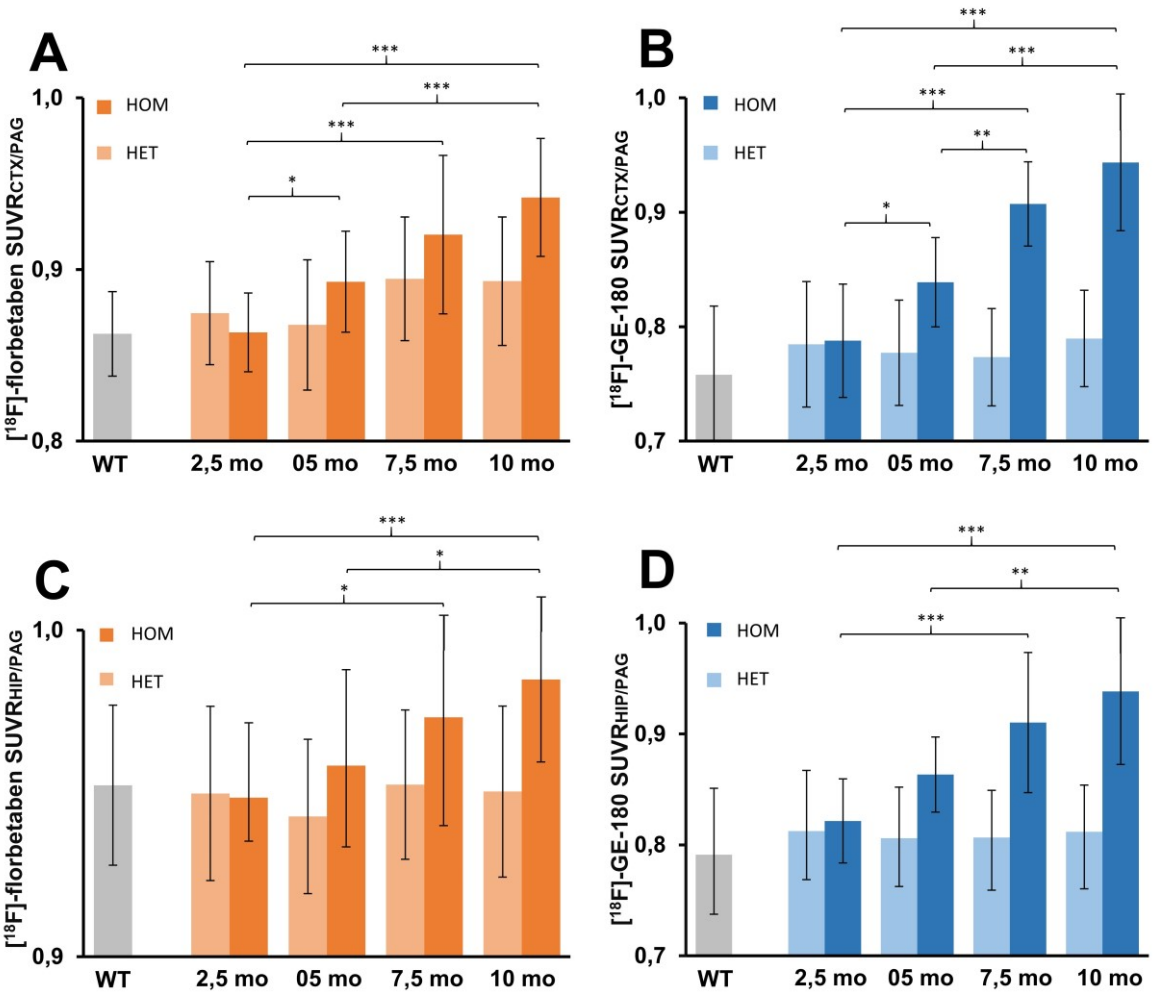

Abbildung 3: Altersabhängigkeit der Aβ- und TSPO-Radiotracer Aufnahme in den frontalen Cortex (CTX) (**A**, **B**) und in den Hippocampus (HIP) (**C**, **D**) von homozygoten (HOM) und heterozygoten (HET) APP-NL-G-F Mäusen. mo = Monate; WT = Wildtyp; *P < 0,05; **P < 0,01; ***P < 0,001.

Darüber hinaus konnte ein signifikanter positiver Zusammenhang zwischen den Amyloid- und den TSPO-PET Ergebnissen sowohl im Bereich des frontalen Cortex (**Abb. 4 A**) als auch im Bereich des Hippocampus (**Abb. 4 B**) gezeigt werden.

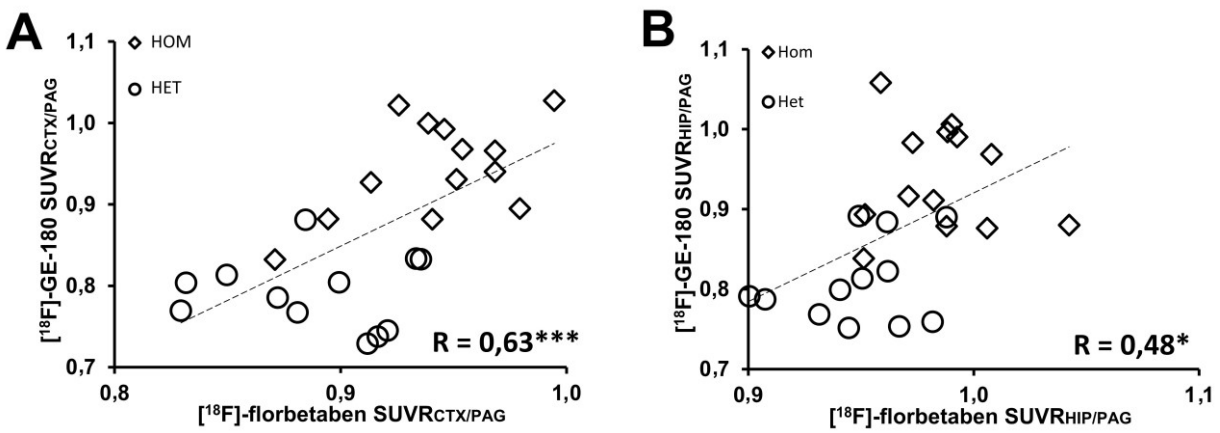

Abbildung 4: Korrelationen zwischen Aβ-Ablagerungen und mikroglialer Aktivierung im Cortex (**A**) und Hippocampus (**B**), gemessen mittels Kleintier PET. HOM = Homozygot; HET = Heterozygot; R = Pearson-Korrelationskoeffizient; *P < 0,05; ***P < 0,001.

Um auch Veränderungen außerhalb der festgelegten Zielvolumina zu detektieren, wurden zusätzlich statische parametrische voxelbasierte Vergleiche mittels SPM 8 (Statistical Parametric Mapping; Wellcome Department of Cognitive Neurology) durchgeführt. Cluster mit signifikant höherer Tracer Aufnahme sowohl von [^{18}F]-florbetaben also auch von [^{18}F]-GE-180 waren in homozygoten APP-NL-G-F Mäusen bereits ab einem Alter von 5 Monaten zu beobachten. β-Amyloid-Ablagerungen zeigten sich hierbei primär ausschließlich im Bereich des linksseitigen Thalamus und später im Alter von 10 Monaten zusätzlich im linksseitigen Cortex **(Abb. 5)**.

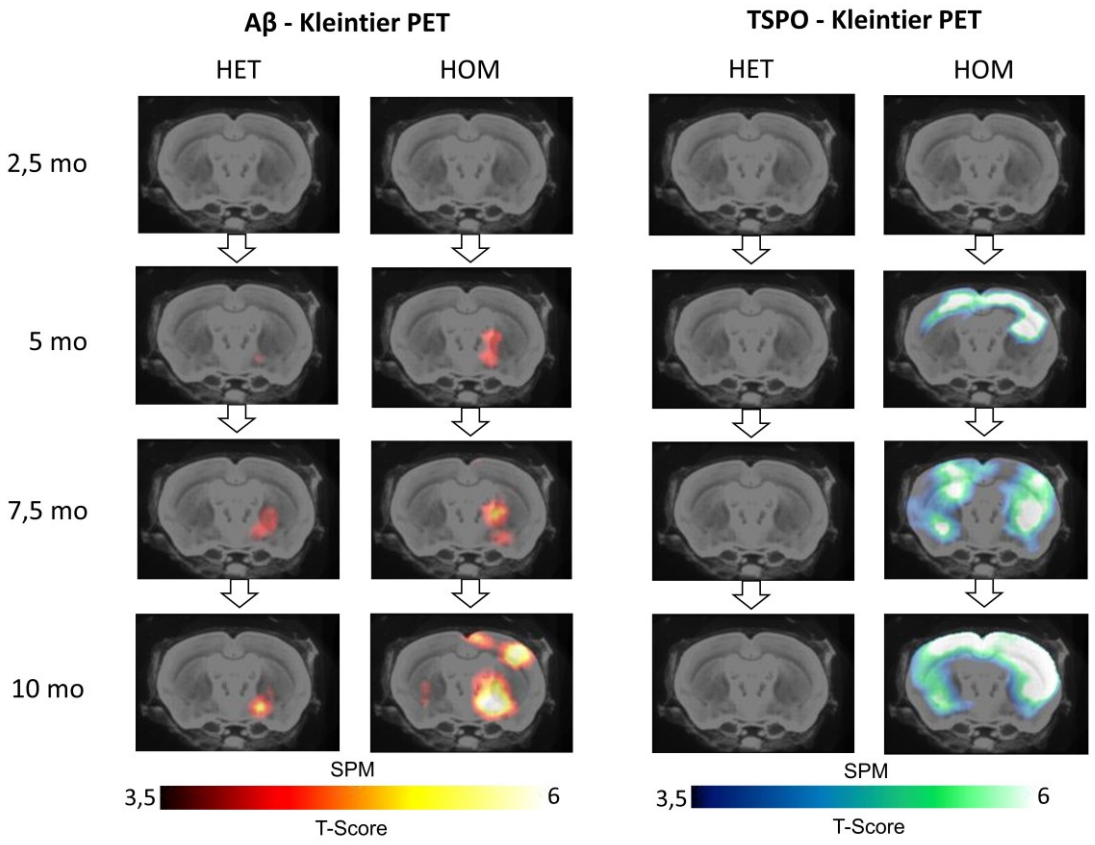

Abbildung 5: Voxelbasierte Analysen der Aβ- und TSPO-Tracer Aufnahme im Gruppenvergleich von homozygoten (HOM) und heterozygoten (HET) APP-NL-G-F Tieren mit altersgleichen Wildtypen zu verschiedenen Alterszeitpunkten. Coronale Schnitte sind auf einen MRT-Atlas des Mausgehirns überlagert. mo = Monate.
Der T-Score kennzeichnet die Abweichung vom Wildtyp-Kollektiv, ein T-Score > 3,5 entspricht dabei einem Signifikanzniveau $p < 0{,}001$ (unkorrigiert für multiples Testen).

Insgesamt wurde ersichtlich, dass das untersuchte knock-in Modell im Vergleich zu transgenen Mausmodellen eine niedrigere [^{18}F]-florbetaben Aufnahme in Relation zu einer stark erhöhten [^{18}F]-GE-180 Aufnahme aufweist. Dies wurde darauf zurückgeführt, dass im Mausmodell APP-NL-G-F ein niedrigerer Anteil des [^{18}F]-florbetaben-affinen fibrillären β-Amyloid in den Plaques gebildet wird. Histochemische Analysen mittels der für fibrilläres β-Amyloid spezifischen Fluoreszenzfärbung Methoxy-X04 und immunhistochemische Analysen mit Hilfe der Gesamt-β-Amyloid

(fibrilläres + nicht-fibrilläres β-Amyloid) nachweisenden Fluoreszenzfärbung NAB228 (Santa Cruz) konnten dies bestätigen (**Abb. 6**).

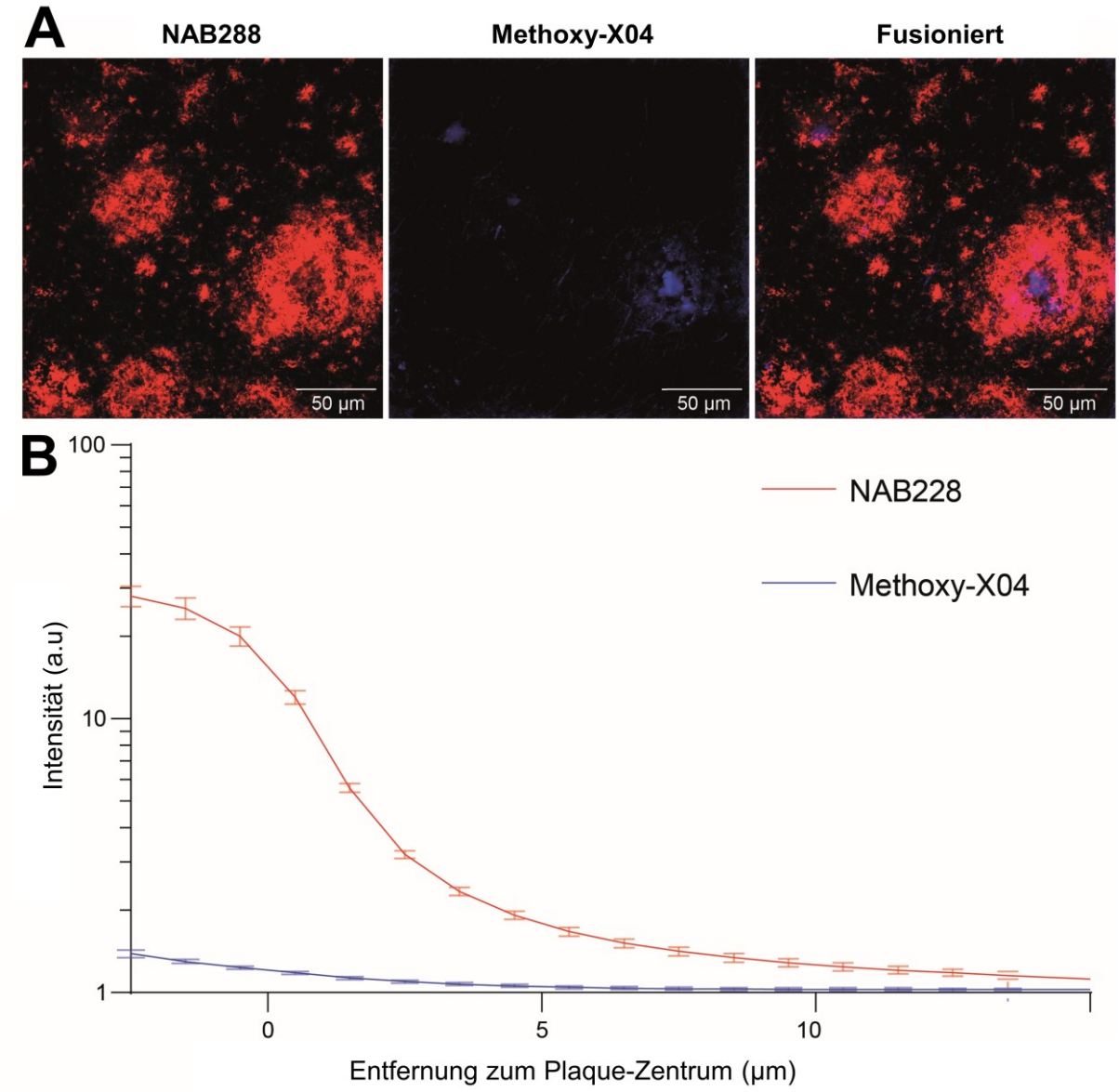

Abbildung 6: A: Geringer Anteil von fibrillärem Aβ (blau, Methoxy-X04) an den gesamten Aβ-Plaques (rot, NAB228). **B**: Graphische Darstellung der mittleren Methoxy-X04 und NAB228 Fluoreszenz-Intensität an den Rändern der Aβ-Plaques. a.u = Absolutwerte.

Im Anschluss an die finalen PET Akquisitionen konnten Verhaltenstests mit Hilfe eines Morris-Wasserlabyrinths durchgeführt werden. 10 Monate alte homozygote APP-NL-

G-F Mäuse wiesen dabei eine signifikant verlängerte Fluchtlatenz im Vergleich zum altersgleichen Wildtyp-Kollektiv auf.

Diese verminderte räumliche Lernfähigkeit steht in einem signifikanten Zusammenhang mit einer erhöhten kortikalen [^{18}F]-GE-180 Aufnahme. Die Ergebnisse der abschließenden (immun)histochemischen und biochemischen Analysen zeigten bei den homozygoten knock-in Mäusen stärker pathologische Werte im Vergleich zum heterozygoten Genotyp und den Wildtypen (**Tab. 1**).

Genotyp (Alter = 10 Monate)			**APP-NL-G-F**				**Wildtyp**	
			Homozygot		**Heterozygot**			
Biochemie	Aβ40 (µg/g)		0,3 ± 0,1***	(n=8)	< 0,1	(n=14)	< 0,1	(n=4)
	Aβ42 (µg/g)		96,9 ± 23,7***	(n=8)	17,6 ± 4,6	(n=14)	0,3 ± 0,2	(n=3)
	sTrem2 (ng/ml)		39,5 ± 4,7***	(n=8)	11,7 ± 2,3	(n=14)	9,5 ± 1,7	(n=4)
(Immun)-histochemie	Methoxy-X04 (%)	CTX	1,3 ± 0,3**	(n=4)	0,4 ± 0,3	(n=5)	Keine Werte	
		HIP	1,4 ± 0,1***	(n=5)	0,1 ± 0,1	(n=5)	Keine Werte	
	Iba1 (%)	CTX	8,5 ± 2,2*	(n=5)	5,1 ± 1,3	(n=5)	4,3 ± 0,9	(n=4)
		HIP	10,0 ± 2,0***	(n=5)	3,3 ± 1,1	(n=5)	2,4 ± 0,8	(n=4)
Verhalten	Fluchtlatenz zur Plattform (s)		29,4 ± 16,8*	(n=11)	20,1 ± 11,7	(n=14)	14,3 ± 4,7	(n=3)

Tabelle 1: Finale multimodale Messwerte homozygoter und heterozygoter APP-NL-G-F Mäuse sowie von Wildtypen. CTX = Cortex; HIP = Hippocampus; *P < 0,05; **P < 0,01; ***P < 0,001.

Zuletzt wurden zwischen allen in dieser Arbeit bestimmten Parametern Korrelationsanalysen durchgeführt. Dabei zeigten die terminalen multimodalen Messwerte exzellente Korrelationen mit den erhobenen SUVR Werten (Alter 10 Monate) (**Abb. 7**).

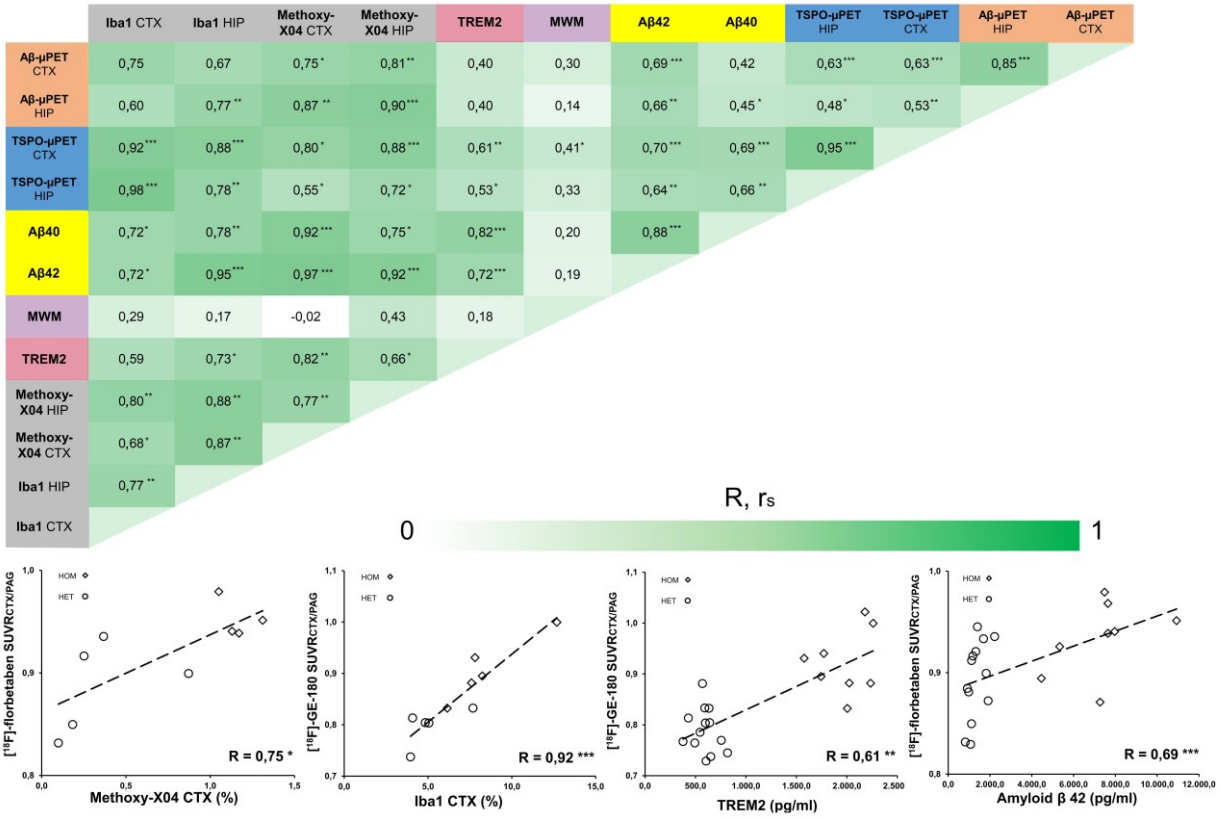

Abbildung 7: Korrelationsanalysen aller terminalen Messparameter. MWM = Morris-Wasserlabyrinth; CTX = Cortex; HIP = Hippocampus; R = Pearson-Korrelationskoeffizient; r_s = Spearman-Korrelationskoeffizient; μPET = Kleintier PET; HOM = Homozygot; HET = Heterozygot; *P < 0,05; **P < 0,01; ***P < 0,001.

Insgesamt wurde ersichtlich, dass die Amyloid- und TSPO-PET Bildgebung bei homozygoten APP-NL-G-F Mäusen erfolgreich zum Monitoring der β-Amyloid-Pathologie und der Neuroinflammation eingesetzt werden kann. Insbesondere in Kombination mit Verhaltenstests lässt sich eine gute Eignung des knock-in Modells für zukünftige longitudinale, mittels Amyloid- und TSPO-PET durchgeführte Medikamentenstudien ableiten.

2.2 Asymmetrie der fibrillären Plaque-Last in Amyloid Mausmodellen

Statische parametrische voxelbasierte Vergleiche im Mausmodell APP-NL-G-F wiesen auf eine linksseitig betonte asymmetrische zerebrale fibrilläre β-Amyloid-Pathologie hin. In Zusammenschau mit häufigen Beobachtungen dieses Phänomens in der klinischen Diagnostik, ergab sich die Grundlage für eine weitere wissenschaftliche Arbeit. Mittels [^{18}F]-florbetaben Amyloid-Kleintier PET sollte das asymmetrische Auftreten von β-Amyloid-Plaques in Amyloid Mausmodellen untersucht werden.

Mit Hilfe einer Querschnittsstudie wurden insgesamt 523 Amyloid-Kleintier PET Scans der transgenen Mausmodelle APP/PS1, PS2APP, APP-SL70 und APPswe sowie des knock-in Modells APP-NL-G-F auf das Vorliegen einer asymmetrischen Neuropathologie analysiert. 27 Amyloid-PET Scans von Wildtypen dienten als Kontrollmaterial. Alle Rohdaten der PET Scans stammten aus vorherigen internen Studien und wurden für diese wissenschaftliche Arbeit standardisiert aufbereitet. Zur Berechnung von SUVR Werten erfolgte zunächst die Normalisierung der Emissionsdateien. Die weiße Substanz diente dabei als Referenzregion für die transgenen Mausmodelle, das periaquäduktale Grau als Pseudoreferenzregion für das knock-in Modell APP-NL-G-F. Als Zielvolumina wurden jeweils bilaterale Regionen im Bereich des Vorderhirns definiert. Die Detektion der Asymmetrie erfolgte mittels Berechnung des Asymmetrie-Index (AI) für die Radiotracer Aufnahme in die jeweilige Vorderhirnhemisphäre mit folgender Formel:

$$AI\ (\%) = 200 \times (L - R) / (L + R).$$

Zunächst mussten für den AI Schwellenwerte definiert werden, ab welchen Amyloid - PET Scans als links- oder rechts-asymmetrisch bewertet werden können. Hierfür wurde jeweils das 95% und 99% Konfidenzintervall (KI) der AI der 27 Amyloid-PET Scans von Wildtypen berechnet (95%-KI_{WT}; 99%-KI_{WT}). Befand sich der AI eines [^{18}F]-florbetaben

Scans der Amyloid Mausmodelle außerhalb der zuvor definierten Konfidenzintervalle, wurde dieser als moderat (>/< 95%-KI_{WT}) oder als stark (>/< 99%-KI_{WT}) asymmetrisch eingestuft.

Insgesamt zeigten dabei 40% (21% links; 19% rechts) der ausgewerteten Amyloid - PET Scans eine moderate und 30% (14% links; 16% rechts) eine stark asymmetrische [^{18}F]-florbetaben Aufnahme ins Gehirn. Eine signifikante altersunabhängige Prädominanz der β-Amyloid-Ablagerungen konnte bei PS2APP Mäusen in der linken Hemisphäre und bei APPswe Mäusen in der rechten Hemisphäre nachgewiesen werden (**Abb. 8**).

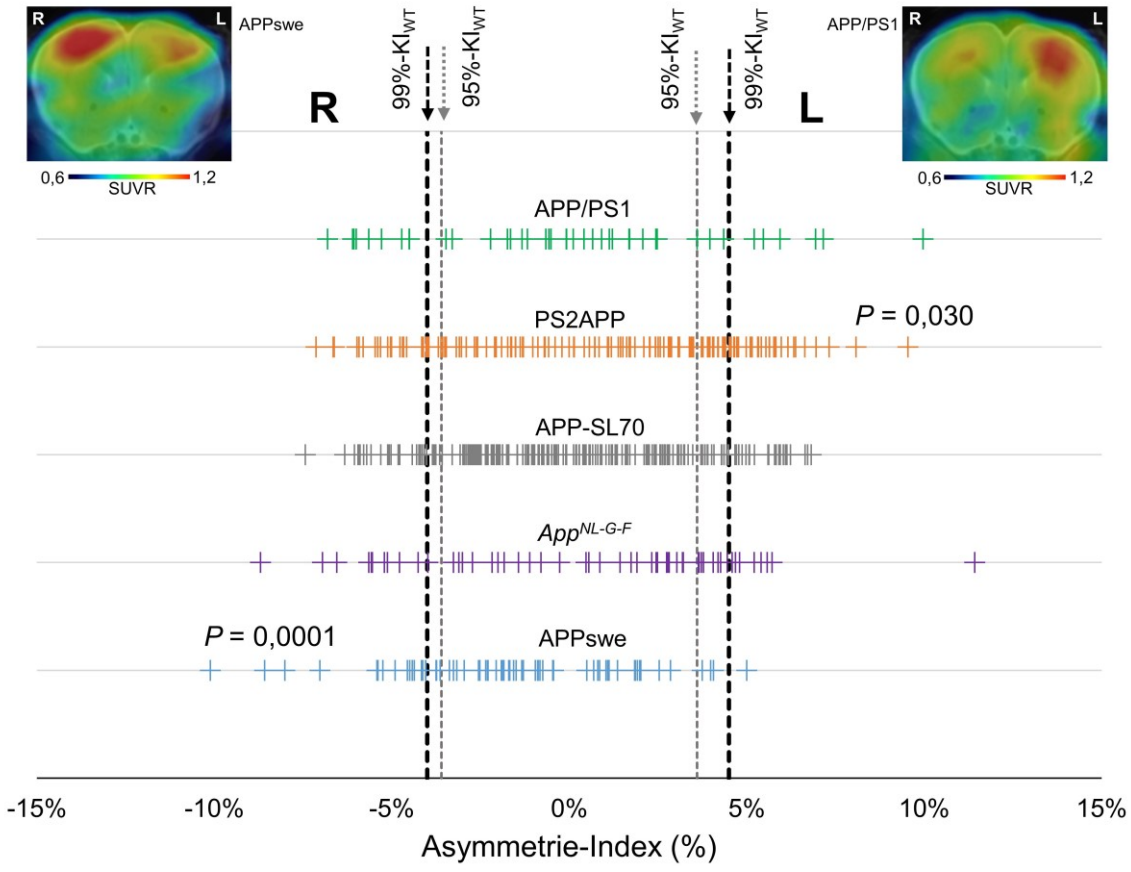

Abbildung 8: Asymmetrie der Aβ-Ablagerungen in Amyloid Mausmodellen. Darstellung der Asymmetrie Indizes aller 523 Aβ-PET Scans als Forest-Plot. Exemplarische SUVR Bilder mit Darstellung einer rechtsseitigen (APPswe) und einer linksseitigen Asymmetrie (APP/PS1). KI = Konfidenzintervall; WT = Wildtyp.

Im nächsten Schritt wurde überprüft, ob ein Zusammenhang zwischen dem Auftreten relevanter Asymmetrien (|AI| > 95%-KI_{WT}) und dem Alter der β-Amyloid akkumulierenden Mäuse besteht. Korrelationsanalysen konnten dabei bei keinem der fünf untersuchten Amyloid Mausmodelle eine signifikante Altersabhängigkeit nachweisen (**Abb. 9**).

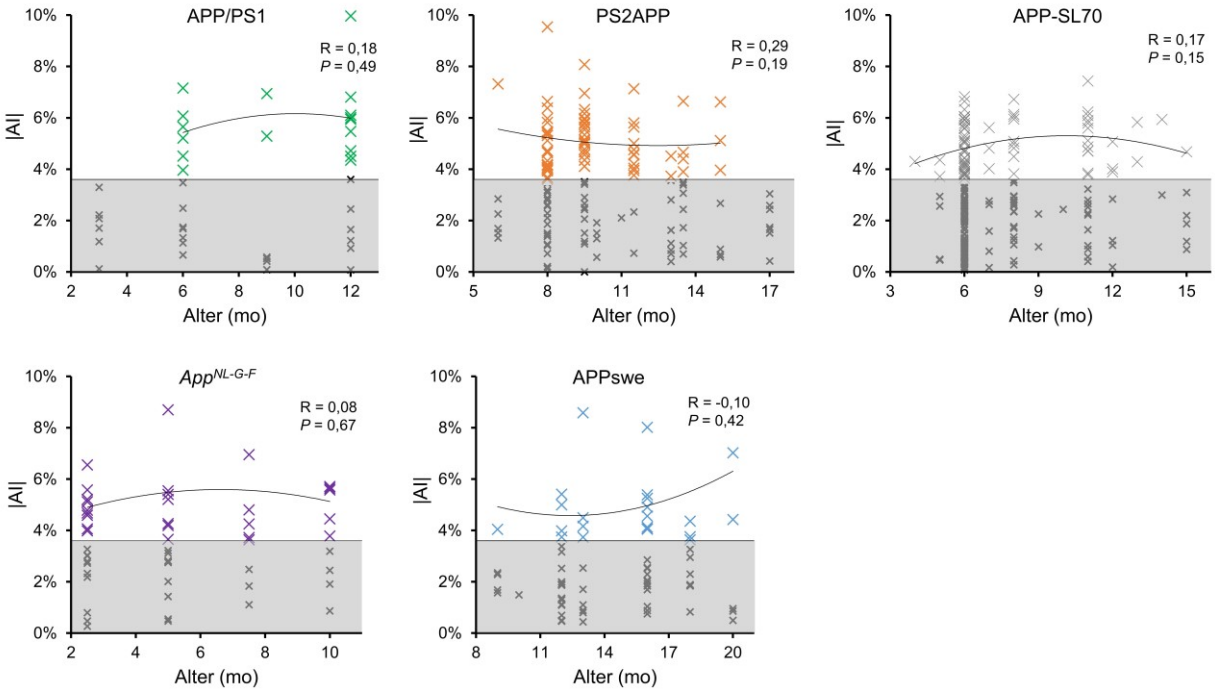

Abbildung 9: Altersabhängigkeit asymmetrischer Aβ-Ablagerungen. Absolutwerte der Asymmetrie Indizes (|AI|) aller Aβ-PET Scans wurden separat für jedes Mausmodell in Abhängigkeit des Alters gesetzt. Symmetrische Werte (|AI| < 95%-KI_{WT}; graue Fläche) wurden für die Korrelationsanalysen exkludiert. mo = Monate; R = Pearson-Korrelationskoeffizient.

Typischerweise wird in präklinischen Studien für histologische und biochemische Analysen je eine Maushirnhemisphäre exploriert. Das häufige Auftreten von β-Amyloid-Asymmetrien in den untersuchten Amyloid Mausmodellen könnte dabei zu einer

erhöhten Varianz in den Messparametern führen. Mittels Korrelationsanalysen konnte ein signifikanter Zusammenhang zwischen erhöhten Variationskoeffizienten des SUVR und einer häufig auftretenden β-Amyloid-Asymmetrie in nach Alter sortierten Gruppen von Amyloid Mäusen nachgewiesen werden (**Abb. 10 A**). Fallzahlanalysen mittels G*Power (Version 3.1.9.2) konnten aufzeigen, dass für einen gewünschten Therapieeffekt von 5% die benötigte Stichprobenzahl bei kombinierter Quantifizierung des SUVR aus beiden Hirnhemisphären niedriger ist, als bei einer Quantifizierung des SUVR aus Einzel-Hemisphären (**Abb. 10 B und C**). Daraus lässt sich schlussfolgern, dass bei histologischen und biochemischen Untersuchungen einzelner Hirnhemisphären höhere Fallzahlen benötigt werden als im Vergleich zur kombinierten Analyse beider Hemisphären, wie es die PET ermöglicht.

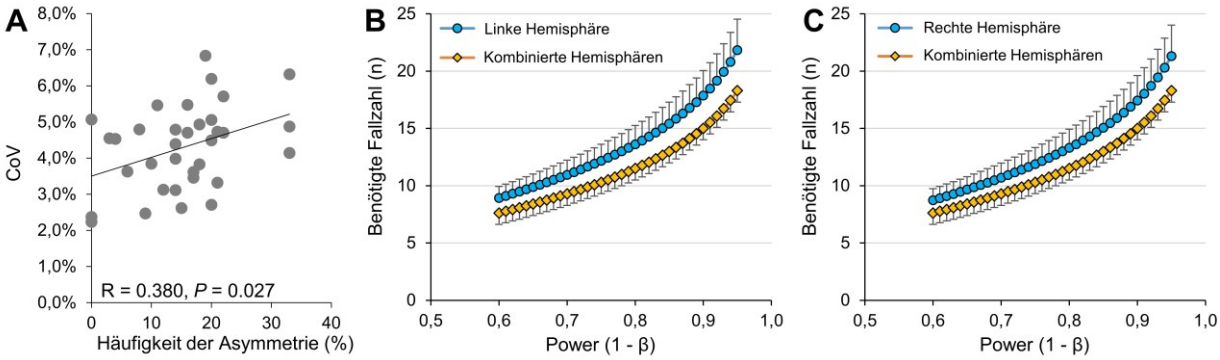

Abbildung 10: A: Zusammenhang zwischen erhöhten Variationskoeffizienten (CoV) des SUVR und einer häufig auftretenden Aβ-Asymmetrie in nach Alter sortierten Gruppen von Amyloid Mäusen. **B und C:** Benötigte Fallzahlen als eine Funktion der statistischen Power für den Vergleich zwischen der kombinierten Quantifizierung des SUVR aus beiden Hirnhemisphären und der Quantifizierung des SUVR aus Einzel-Hemisphären. R = Pearson-Korrelationskoeffizient.

Abschließend wurden in dieser Arbeit Korrelationsanalysen zwischen den Asymmetrie Indizes von jeweils 136 Amyloid- und TSPO-Kleintier PET Scans der Amyloid

Mausmodelle APP/PS1, PS2APP, APP-SL70 und APP-NL-G-F durchgeführt. In jedem der vier untersuchten Modelle konnte dabei ein signifikanter Zusammenhang zwischen asymmetrischer β-Amyloid-Pathologie und einer ipsilateralen Neuroinflammation nachgewiesen werden (**Abb. 11**).

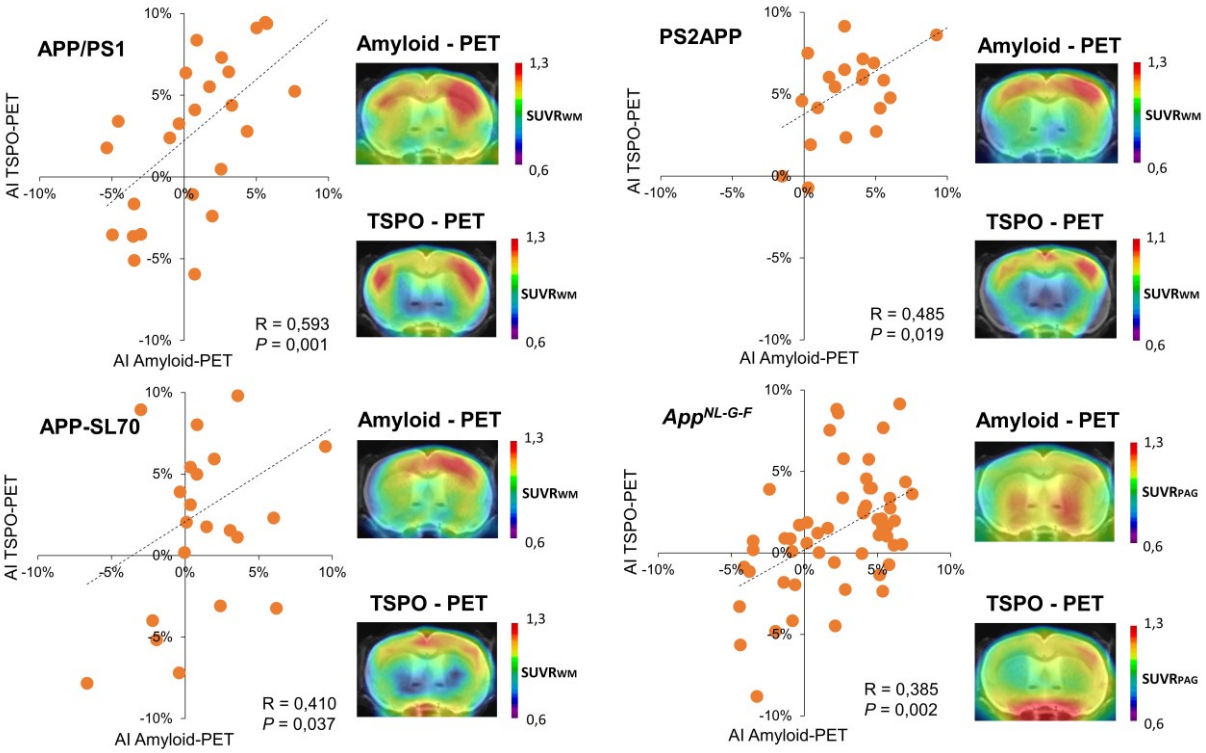

Abbildung 11: Zusammenhang zwischen asymmetrischen Aβ-Ablagerungen und ipsilateraler mikroglialer Aktivierung. Korrelationen zwischen den Asymmetrie Indizes (AI) von Aβ- und TSPO-PET in den Mausmodellen APP/PS1, PS2APP, APP-SL70 und APP-NL-G-F zeigten eine kongruente Asymmetrie für beide Biomarker. PAG = Periaqueduktales Grau; WM = Weiße Substanz; R = Pearson-Korrelationskoeffizient.

Zusammengefasst lässt sich festhalten, dass fast ein Drittel aller untersuchten Amyloid Mäuse eine stark asymmetrische β-Amyloid-Pathologie aufwiesen. Dies sollte bei der Planung zukünftiger präklinischer Studien mitberücksichtigt werden. Insbesondere bei ex vivo Untersuchungen einzelner Hirnhemisphären könnten sich Asymmetrien als potentielle Störfaktoren bemerkbar machen. Eine fehlende Altersabhängigkeit des

Auftretens relevanter β-Amyloid-Asymmetrien lässt vermuten, dass der Entstehung einer lateralisierten β-Amyloid-Pathologie genetische Faktoren unterliegen. Der signifikante Zusammenhang zwischen asymmetrischer fibrillärer Plaque-Last und ipsilateraler Neuroinflammation bestärkt die gängige Hypothese, dass die Migration und Aktivierung von Mikroglia als immunologische Antwort auf zerebrale β-Amyloid-Ablagerungen erfolgt.

3. Zusammenfassung

Die nicht physiologische Überexpression des β-Amyloid (Aβ) Vorläufer Proteins (engl.: Amyloid Precursor Protein, APP) in den bisher etablierten transgenen Amyloid-Mausmodellen der Alzheimer Erkrankung kann in präklinischen Studien zu potenziellen Störfaktoren führen. Das neue Mausmodell APP-NL-G-F enthält ein mutiertes knock-in Konstrukt, wodurch es möglicherweise ein verbessertes Modell der Alzheimer Krankheit für β-Amyloid-fokussierte Behandlungsstudien darstellt. Ziel dieser Doktorarbeit war es, die serielle Kleintier Positronen-Emissions-Tomographie (PET) der β-Amyloidose und Neuroinflammation bei APP-NL-G-F-Mäusen für zukünftige Therapieüberwachungsstudien zu etablieren und zu validieren.

Asymmetrien der β-Amyloid-Plaque-Last sind ein bekanntes Phänomen bei klinischen PET-Untersuchungen der Alzheimer Krankheit, wohingegen sie in Amyloid Mausmodellen bisher nicht genauer untersucht wurden. Daher ergab sich als zweites Ziel dieser Doktorarbeit Asymmetrien der β-Amyloid Pathologie in Amyloid Mausmodellen durch Amyloid-Kleintier PET zu untersuchen. Zusätzlich wurde überprüft, ob diese Asymmetrien mit einer mikroglialen Aktivierung assoziiert sind.

41 APP-NL-G-F-Mäuse (20 Homozygote und 21 Heterozygote) und 12 altersgleiche Wildtypen wurden im Alter von 2,5 bis 10 Monaten mittels [^{18}F]-florbetaben Amyloid-PET und [^{18}F]-GE-180 18-kDa Translokatorprotein (TSPO)-PET in einem longitudinalen Studiendesign untersucht. Für Amyloid- und TSPO-PET wurden relative Standard-Aufnahmewerte (engl.: Standardized-Uptake-Value-Ratio, SUVR) für Cortex und Hippocampus berechnet. Die voxelweise Analyse der SUVR-Bilder erfolgte mittels statistisch parametrischem Mapping. Alle Mäuse durchliefen nach ihrem letzten PET Scan einen Test für die räumliche Lernfähigkeit mit Hilfe eines Morris-Wasserlabyrinths. Die abschließende Quantifizierung von fibrillärem β-Amyloid und

aktivierter Mikroglia durch (Immun)histochemie und Biochemie diente zur Validierung der PET Ergebnisse.

Im Rahmen der zweiten wissenschaftlichen Arbeit wurden 523 Amyloid-PET Scans von fünf verschiedenen Amyloid Mausmodellen (APP/PS1, PS2APP, APP-SL70, APP-NL-G-F und APPswe) zusammen mit 136 TSPO-PET Scans zum Nachweis mikroglialer Aktivierung im Rahmen einer Querschnittsstudie analysiert. Alle PET-Rohdaten stammten aus früheren internen Studien und wurden für diese Arbeit neu aufbereitet. Zwei bilaterale Zielvolumina im Bereich des Vorderhirns wurden für die Berechnung von SUVRs verwendet. Bei transgenen Mausmodellen diente die weiße Substanz als Referenzregion, bei dem knock-in Modell APP-NL-G-F wurde das periaquäduktale Grau als Pseudoreferenzregion gewählt. Aus der unterschiedlichen Traceraufnahme in die jeweiligen Hirnhemisphären wurde der Asymmetrie Index berechnet. Die hochgerechneten erforderlichen Stichprobengrößen wurden zwischen Analysen einzelner und kombinierter Hirnhemisphären verglichen. Abschließend erfolgten Korrelationsanalysen zwischen den Amyloid-PET Asymmetrie Indizes und den TSPO-PET Asymmetrie Indizes.

Die ubiquitäre Amyloid-Pathologie im Gehirn der APP-NL-G-F Mäuse erschwerte die Verwendung von zuvor etablierten Referenzregionen, wie dem Kleinhirn oder der weißen Substanz. Unter Verwendung einer Varianzanalyse für beide PET-Tracer zusammen mit (immun)histochemischen Analysen erwies sich das periaqueduktale Grau im Mesencephalon als eine geeignete Pseudo-Referenzregion für beide Tracer. Homozygote APP-NL-G-F-Mäuse wiesen in einem Altersintervall von 7,5 Monaten (10 Monate vs. 2,5 Monate) für Amyloid- (+9,1%; +3,8%) und TSPO-PET (+19,8%; +14,2%) ansteigende SUVRs im Cortex und Hippocampus auf (alle $P < 0,05$). Heterozygote APP-NL-G-F-Mäuse zeigten keine signifikanten Veränderungen mit

zunehmendem Alter. Ein signifikanter positiver Zusammenhang zwischen den Amyloid- und den TSPO-PET Ergebnissen wurde sowohl im Cortex ($R = 0,64$; $P < 0,001$) als auch im Hippocampus ($R = 0,48$; $P < 0,05$) beobachtet. Erste signifikante Cluster von β-Amyloid-Ablagerungen und mikroglialer Aktivierung konnten bei homozygoten Mäusen im Alter von 5 Monaten mittels der sensitiveren voxelweisen Analyse detektiert werden. (Immun)histochemische Analysen zeigten in den Plaques von APP-NL-G-F-Mäusen im Vergleich zu anderen transgenen Amyloid Mausmodellen einen geringeren Anteil an fibrillärem β-Amyloid. Bei 10 Monate alten homozygoten APP-NL-G-F-Mäusen war die Fluchtlatenzzeit im Wasserlabyrinth im Vergleich zu Wildtypen signifikant erhöht und ging mit einer erhöhten kortikalen TSPO-Radiotracer Aufnahme einher. Die terminalen (immun)histochemischen und biochemischen Messparameter korrelierten stark mit den erhobenen PET-Daten.

Zur Detektion relevanter Asymmetrien erfolgte zunächst die Definition von Schwellenwerten auf der Grundlage von PET-Messungen bei Wildtypen. Mittels dieser Methodik wurden in mindestens 30% aller untersuchten Amyloid Mausmodelle stark asymmetrische β-Amyloid-Ablagerungen identifiziert, jedoch mit unterschiedlichem Ausmaß und unterschiedlicher Prädilektion der Lateralisation. Asymmetrien waren mit einer höheren Varianz der Traceraufnahme in den einzelnen Hemisphären verbunden. Dies resultierte in einer höheren erforderlichen Stichprobengröße für die Analyse einzelner Hemisphären im Gegensatz zur kombinierten Messung beider Hirnhemisphären. In keinem der untersuchten Amyloid Mausmodelle konnte ein Zusammenhang zwischen asymmetrischer β-Amyloid-Verteilung und dem Alter der Tiere nachgewiesen werden. In ähnlich starkem Ausmaß (alle $R > 0,385$, alle $P < 0,05$) korrelierte die Lateralisation der Amyloid-PET Daten mit der Lateralisation der TSPO-PET Daten in vier untersuchten Amyloid Mausmodellen.

Die Bildgebung von APP-NL-G-F-Mäusen mittels Amyloid- und TSPO-PET wird durch eine ubiquitär zerebrale β-Amyloid-Pathologie und eine relativ geringe Fibrillarität der β-Amyloid-Plaques erschwert. Unter Verwendung des periaqueduktialen Graus als Pseudo-Referenzregion ist diese jedoch erfolgreich durchführbar. Die Progression der Alzheimer Neuropathologie kann durch die serielle [^{18}F]-florbetaben und [^{18}F]-GE-180 PET in homozygoten APP-NL-G-F-Mäusen sensitiv detektiert werden, während beim heterozygoten Genotyp nur geringfügige Veränderungen nachweisbar sind. Die kombinierte Anwendung der PET zusammen mit Verhaltenstests im neuen knock-in Alzheimer Mausmodell APP-NL-G-F stellt eine vielversprechende Methode zur präklinischen Evaluierung neuer Therapeutika dar.

Asymmetrien der fibrillären Plaque-Neuropathologie konnten in Amyloid Mausmodellen mit einer hohen Häufigkeit nachgewiesen werden. Dieses Phänomen muss bei der Planung und Gestaltung präklinischer Studien berücksichtigt werden, insbesondere wenn einzelne Hemisphären mit ex vivo Methoden untersucht werden. Die fehlende Altersabhängigkeit der asymmetrischen β-Amyloid-Verteilung impliziert, dass genetische Faktoren bei der Entwicklung einer lateralisierten β-Amyloidose bei Alzheimer Mausmodellen zugrunde liegen. Eine begleitende Asymmetrie der mikroglialen Aktivierung weist auf eine neuroinflammatorische Komponente bei der Prädominanz der fibrillären Amyloidose in der jeweiligen Hemisphäre hin.

4. Summary

Overexpression of β-amyloid (Aβ) precursor protein (APP) in previously established transgenic amyloid mouse models of Alzheimer's disease may lead to potential confounders in preclinical studies. The new mouse model APP-NL-G-F contains a mutated knock-in construct, potentially making it an improved model of Alzheimer's

disease for β-amyloid-focused treatment studies. The aim of this dissertation was to establish and validate serial small animal positron emission tomography (PET) imaging of β-amyloidosis and neuroinflammation in APP-NL-G-F mice for future therapy monitoring trials.

Asymmetries of β-amyloid plaque burden are a well-known phenomenon in clinical PET studies of Alzheimer's disease, whereas they have not been studied in detail in amyloid mouse models. Therefore, the investigation of asymmetries of β-amyloid pathology in amyloid mouse models by amyloid small animal PET, arose as a second objective of this dissertation. Furthermore, experiments of the thesis examined whether these asymmetries are associated with microglial activation.

41 APP-NL-G-F mice (20 homozygous and 21 heterozygous) and 12 age-matched wild-type animals were studied from 2.5 to 10 months of age by [^{18}F]-florbetaben amyloid PET and [^{18}F]-GE-180 18-kDa translocator protein (TSPO) PET in a longitudinal study design. Target-to-reference-tissue standardized uptake value ratios (SUVRs) were calculated for amyloid and TSPO PET for cortex and hippocampus. Statistical parametric mapping was used to perform voxelwise analysis of SUVR images. All mice underwent a spatial learning ability test using a Morris water maze after their final PET scan. Validation of the PET results took place by means of terminal quantification of fibrillar β-amyloid and activated microglia by (immuno)histochemistry and biochemistry.

To accomplish the second aim of the thesis, 523 amyloid PET scans of five different amyloid mouse models (APP/PS1, PS2APP, APP-SL70, APP-NL-G-F and APPswe) together with 136 TSPO PET scans for microglial activation were analyzed cross-sectionally. All raw PET data originated from previous in-house studies and were reprocessed in standardized way for this study. Two bilateral volumes of interest in the

somatomotor cortex were used for calculation of the forebrain–to–white matter SUVR (transgenic mouse models) or the forebrain–to–periaqueductal gray SUVR (knock-in mouse model). The asymmetry index was calculated from the difference in tracer uptake in the respective brain hemispheres. Extrapolated required sample sizes were compared between analyses of single and combined cerebral hemispheres. Asymmetry indices of amyloid PET were analyzed in correlation with TSPO PET asymmetry indices.

The widespread amyloid pathology in the brain of APP-NL-G-F mice made it difficult to use previously established reference regions, such as the cerebellum or white matter. Using analysis of variance for each PET tracer together with (immuno)histochemical analyses, the periaqueductal gray in the mesencephalon proved to be a suitable pseudo-reference region for each tracer. Homozygous APP-NL-G-F mice showed increasing SUVRs in the cortex and hippocampus at an age interval of 7.5 months (10 months vs. 2.5 months) for amyloid (+9.1%; +3.8%) and TSPO PET (+19.8%; +14.2%) (all $P < 0.05$). Heterozygous APP-NL-G-F mice did not show rising SUVRs with age. A significant positive correlation between amyloid and TSPO PET results was observed in both cortex ($R = 0.64$; $P < 0.001$) and hippocampus ($R = 0.48$; $P < 0.05$). First significant clusters of β-amyloid deposition and microglial activation were detected in homozygous mice at 5 months of age using the more sensitive voxel-wise analysis. (Immuno)histochemical analysis revealed a lower fraction of [^{18}F]-florbetaben-affine fibrillar β-amyloid in the plaques of knock-in mice compared to other transgenic amyloid mouse models. In 10 month old homozygous APP-NL-G-F mice, escape latency in the water maze was significantly increased compared with wild-type mice and was associated with increased cortical TSPO radiotracer uptake. Terminal

(immuno)histochemical and biochemical measurement parameters correlated strongly with the collected PET data.

After defining an asymmetry threshold based on PET measurements in wild-type mice, relevant asymmetries of β-amyloid deposition were identified in at least 30% of all studied amyloid mouse models, but with different magnitudes and side predilections. Asymmetries were associated with higher variance in tracer uptake in each hemisphere. This resulted in a higher required sample size for single hemisphere analysis as opposed to combined measurement of both cerebral hemispheres. There was no significant association between age and asymmetric β-amyloid distribution in any amyloid mouse model. Lateralization of amyloid PET was significant correlating with contemporaneous TSPO PET data in four investigated amyloid mouse models with a similar strong magnitude (all $R > 0.385$, all $P < 0.05$).

Imaging of APP-NL-G-F mice by amyloid and TSPO PET is complicated by ubiquitous cerebral β-amyloid pathology and low fibrillarity of β-amyloid plaques. However, using the periaqueductal gray as a pseudo-reference region, it is successfully feasible. Progression of AD neuropathology can be sensitively detected by serial [^{18}F]-florbetaben and [^{18}F]-GE-180 PET in homozygous APP-NL-G-F mice, whereas only minor changes are detectable in the heterozygous genotype. The combined use of PET together with behavioral testing in the new knock-in Alzheimer mouse model APP-NL-G-F represents a promising method for preclinical evaluation of new therapeutics.

Asymmetries of fibrillar plaque burden were detected with a high frequency in amyloid mouse models. This phenomenon is neglected in most current studies on amyloid mice and calls for consideration in the planning and design of preclinical trials, especially when only one hemisphere is investigated by methods ex vivo. The lack of age dependency on asymmetric β-amyloid distribution implies that genetic factors underlie

the development of lateralized amyloidosis in Alzheimer model mice. Concomitant asymmetries of microglial activation suggest a neuroinflammatory constituent in the predominance of fibrillary amyloidosis in each hemisphere.

5. Literaturverzeichnis

Barthel, H. and O. Sabri (2011). "Florbetaben to trace amyloid-beta in the Alzheimer brain by means of PET." J Alzheimers Dis **26 Suppl 3**: 117-121.

Bateman, R. J., C. Xiong, et al. (2012). "Clinical and biomarker changes in dominantly inherited Alzheimer's disease." N Engl J Med **367**(9): 795-804.

Blume, T., C. Focke, et al. (2018). "Microglial response to increasing amyloid load saturates with aging: a longitudinal dual tracer in vivo muPET-study." J Neuroinflammation **15**(1): 307.

Braak, H. and E. Braak (1991). "Neuropathological stageing of Alzheimer-related changes." Acta Neuropathol **82**(4): 239-259.

Brendel, M., F. Probst, et al. (2016). "Glial Activation and Glucose Metabolism in a Transgenic Amyloid Mouse Model: A Triple-Tracer PET Study." J Nucl Med **57**(6): 954-960.

Cagnin, A., D. J. Brooks, et al. (2001). "In-vivo measurement of activated microglia in dementia." Lancet **358**(9280): 461-467.

Citron, M., T. Oltersdorf, et al. (1992). "Mutation of the beta-amyloid precursor protein in familial Alzheimer's disease increases beta-protein production." Nature **360**(6405): 672-674.

Clark, C. M., J. A. Schneider, et al. (2011). "Use of florbetapir-PET for imaging beta-amyloid pathology." JAMA **305**(3): 275-283.

Cuyvers, E. and K. Sleegers (2016). "Genetic variations underlying Alzheimer's disease: evidence from genome-wide association studies and beyond." Lancet Neurol **15**(8): 857-868.

Dubois, B., A. Padovani, et al. (2016). "Timely Diagnosis for Alzheimer's Disease: A Literature Review on Benefits and Challenges." J Alzheimers Dis **49**(3): 617-631.

Edison, P., C. K. Donat and M. Sastre (2018). "In vivo Imaging of Glial Activation in Alzheimer's Disease." Front Neurol **9**: 625.

Egan, M. F., J. Kost, et al. (2018). "Randomized Trial of Verubecestat for Mild-to-Moderate Alzheimer's Disease." N Engl J Med **378**(18): 1691-1703.

Focke, C., T. Blume, et al. (2019). "Early and Longitudinal Microglial Activation but Not Amyloid Accumulation Predicts Cognitive Outcome in PS2APP Mice." J Nucl Med **60**(4): 548-554.

Fodero-Tavoletti, M. T., D. Brockschnieder, et al. (2012). "In vitro characterization of [18F]-florbetaben, an Abeta imaging radiotracer." Nucl Med Biol **39**(7): 1042-1048.

Frings, L., S. Hellwig, et al. (2015). "Asymmetries of amyloid-beta burden and neuronal dysfunction are positively correlated in Alzheimer's disease." Brain **138**(Pt 10): 3089-3099.

Goertzen, A. L., Q. Bao, et al. (2012). "NEMA NU 4-2008 comparison of preclinical PET imaging systems." J Nucl Med **53**(8): 1300-1309.

Hardy, J. and D. Allsop (1991). "Amyloid deposition as the central event in the aetiology of Alzheimer's disease." Trends Pharmacol Sci **12**(10): 383-388.

Heneka, M. T., M. J. Carson, et al. (2015). "Neuroinflammation in Alzheimer's disease." Lancet Neurol **14**(4): 388-405.

Hsiao, K. (1998). "Transgenic mice expressing Alzheimer amyloid precursor proteins." Exp Gerontol **33**(7-8): 883-889.

Jack, C. R., Jr., D. A. Bennett, et al. (2018). "NIA-AA Research Framework: Toward a biological definition of Alzheimer's disease." Alzheimers Dement **14**(4): 535-562.

Kim, J., L. Onstead, et al. (2007). "Abeta40 inhibits amyloid deposition in vivo." J Neurosci **27**(3): 627-633.

Lichtenthaler, S. F., R. Wang, et al. (1999). "Mechanism of the cleavage specificity of Alzheimer's disease gamma-secretase identified by phenylalanine-scanning mutagenesis of the transmembrane domain of the amyloid precursor protein." Proc Natl Acad Sci U S A **96**(6): 3053-3058.

Masuda, A., Y. Kobayashi, et al. (2016). "Cognitive deficits in single App knock-in mouse models." Neurobiol Learn Mem **135**: 73-82.

Nilsson, P., T. Saito and T. C. Saido (2014). "New mouse model of Alzheimer's." ACS Chem Neurosci **5**(7): 499-502.

Ossenkoppele, R., D. R. Schonhaut, et al. (2016). "Tau PET patterns mirror clinical and neuroanatomical variability in Alzheimer's disease." Brain **139**(Pt 5): 1551-1567.

Palmqvist, S., P. S. Insel, et al. (2019). "Cerebrospinal fluid and plasma biomarker trajectories with increasing amyloid deposition in Alzheimer's disease." EMBO Mol Med **11**(12): e11170.

Pardridge, W. M. (2020). "Treatment of Alzheimer's Disease and Blood-Brain Barrier Drug Delivery." Pharmaceuticals (Basel) **13**(11).

Parhizkar, S., T. Arzberger, et al. (2019). "Loss of TREM2 function increases amyloid seeding but reduces plaque-associated ApoE." Nat Neurosci **22**(2): 191-204.

Puzzo, D., W. Gulisano, et al. (2015). "Rodent models for Alzheimer's disease drug discovery." Expert Opin Drug Discov **10**(7): 703-711.

Querfurth, H. W. and F. M. LaFerla (2010). "Alzheimer's disease." N Engl J Med **362**(4): 329-344.

Rominger, A., M. Brendel, et al. (2013). "Longitudinal assessment of cerebral beta-amyloid deposition in mice overexpressing Swedish mutant beta-amyloid precursor protein using 18F-florbetaben PET." J Nucl Med **54**(7): 1127-1134.

Rominger, A., E. Mille, et al. (2010). "Validation of the octamouse for simultaneous 18F-fallypride small-animal PET recordings from 8 mice." J Nucl Med **51**(10): 1576-1583.

Sabbagh, M. N. and J. Cummings (2020). "Open Peer Commentary to "Failure to demonstrate efficacy of aducanumab: An analysis of the EMERGE and ENGAGE Trials as reported by Biogen December 2019"." Alzheimers Dement.

Saito, T., Y. Matsuba, et al. (2014). "Single App knock-in mouse models of Alzheimer's disease." Nat Neurosci **17**(5): 661-663.

Salloway, S., R. Sperling, et al. (2014). "Two phase 3 trials of bapineuzumab in mild-to-moderate Alzheimer's disease." N Engl J Med **370**(4): 322-333.

Sasaguri, H., P. Nilsson, et al. (2017). "APP mouse models for Alzheimer's disease preclinical studies." EMBO J **36**(17): 2473-2487.

Schneider, L. S. (2013). "Alzheimer disease pharmacologic treatment and treatment research." Continuum (Minneap Minn) **19**(2 Dementia): 339-357.

Sebastian Monasor, L., S. A. Muller, et al. (2020). "Fibrillar Abeta triggers microglial proteome alterations and dysfunction in Alzheimer mouse models." Elife **9**.

Sepulcre, J., M. R. Sabuncu, et al. (2013). "In vivo characterization of the early states of the amyloid-beta network." Brain **136**(Pt 7): 2239-2252.

Tetzloff, K. A., J. Graff-Radford, et al. (2018). "Regional Distribution, Asymmetry, and Clinical Correlates of Tau Uptake on [18F]AV-1451 PET in Atypical Alzheimer's Disease." J Alzheimers Dis **62**(4): 1713-1724.

Tsubuki, S., Y. Takaki and T. C. Saido (2003). "Dutch, Flemish, Italian, and Arctic mutations of APP and resistance of Abeta to physiologically relevant proteolytic degradation." Lancet **361**(9373): 1957-1958.

Vandenberghe, R., K. Van Laere, et al. (2010). "18F-flutemetamol amyloid imaging in Alzheimer disease and mild cognitive impairment: a phase 2 trial." Ann Neurol **68**(3): 319-329.

Webster, S. J., A. D. Bachstetter, et al. (2014). "Using mice to model Alzheimer's dementia: an overview of the clinical disease and the preclinical behavioral changes in 10 mouse models." Front Genet **5**: 88.

Winblad, B., P. Amouyel, et al. (2016). "Defeating Alzheimer's disease and other dementias: a priority for European science and society." Lancet Neurol **15**(5): 455-532.

Zanotti-Fregonara, P., B. Pascual, et al. (2018). "Head-to-Head Comparison of (11)C-PBR28 and (18)F-GE180 for Quantification of the Translocator Protein in the Human Brain." J Nucl Med **59**(8): 1260-1266.

Ziegler-Graham, K., R. Brookmeyer, et al. (2008). "Worldwide variation in the doubling time of Alzheimer's disease incidence rates." Alzheimers Dement **4**(5): 316-323.

Zimmer, E. R., M. J. Parent, et al. (2014). "MicroPET imaging and transgenic models: a blueprint for Alzheimer's disease clinical research." Trends Neurosci **37**(11): 629-641.

6. Danksagung

Meinem Doktorvater Herrn Priv.-Doz. Dr. med. Matthias Brendel von der Klinik und Poliklinik für Nuklearmedizin der Universität München danke ich für die exzellente Betreuung dieser wissenschaftlichen Arbeit. Mit seiner eigenen Begeisterung für die Alzheimer Forschung motivierte er mich stets aufs Neue, mich noch tiefer mit der Thematik zu befassen und stand mir bei allen Fragestellungen jederzeit professionell und freundschaftlich zu Rate.

Herrn Prof. Dr. med. Peter Bartenstein und Herrn Prof. Dr. med. Axel Rominger möchte ich für die Ermöglichung dieses Projektes danken.

Maximilian Deußing und Carola Focke danke ich für die hervorragende Einarbeitung in die Laborarbeit sowie in die Auswertungs-Algorithmen. Bei meinem Doktorandenkollegen Florian Eckenweber möchte ich mich für die kompetente Zusammenarbeit und gegenseitige Unterstützung bei den einzelnen Projekten bedanken.

Darüber hinaus danke ich Karin Bormann-Giglmaier und Rosel Oos für die stets hervorragende Zusammenarbeit und die harmonische Atmosphäre bei der Durchführung der Experimente.

Mein tiefster Dank gilt meinen Eltern und meiner Freundin Lena, die mich in allen schwierigen Lebenslagen emotional unterstützten und mir immer halfen meine Ziele im Auge zu behalten. Abschließend danke ich noch meinen Vierbeinern Bella und Oscar, die allzeit bereit waren mit mir spazieren zu gehen und mir damit halfen stets einen klaren Kopf zu behalten.

Longitudinal PET Monitoring of Amyloidosis and Microglial Activation in a Second-Generation Amyloid-β Mouse Model

Christian Sacher*[1], Tanja Blume*[1,2], Leonie Beyer*[1], Finn Peters[2], Florian Eckenweber[1], Carmelo Sgobio[2], Maximilian Deussing[1], Nathalie L. Albert[1], Marcus Unterrainer[1], Simon Lindner[1], Franz-Josef Gildehaus[1], Barbara von Ungern-Sternberg[1], Irena Brzak[3], Ulf Neumann[3], Takashi Saito[4], Takaomi C. Saido[4], Peter Bartenstein[1], Axel Rominger[1,5,6], Jochen Herms*[2,5,7], and Matthias Brendel*[1,5]

[1]*Department of Nuclear Medicine, University Hospital of Munich, LMU Munich, Munich Germany;* [2]*DZNE–German Center for Neurodegenerative Diseases, Munich, Germany;* [3]*Neuroscience, Novartis Institutes for BioMedical Research (NIBR), Basel, Switzerland;* [4]*Laboratory for Proteolytic Neuroscience, RIKEN Center for Brain Science, Saitama, Japan;* [5]*Munich Cluster for Systems Neurology (SyNergy), Munich, Germany;* [6]*Department of Nuclear Medicine, Inselspital, University Hospital Bern, Bern, Switzerland; and* [7]*Center of Neuropathology and Prion Research, University of Munich, Munich, Germany*

Nonphysiologic overexpression of amyloid-β (Aβ) precursor protein in common transgenic Aβ mouse models of Alzheimer disease likely hampers their translational potential. The novel $App^{NL\text{-}G\text{-}F}$ mouse incorporates a mutated knock-in, potentially presenting an improved model of Alzheimer disease for Aβ-targeting treatment trials. We aimed to establish serial small-animal PET of amyloidosis and neuroinflammation in $App^{NL\text{-}G\text{-}F}$ mice as a tool for therapy monitoring. **Methods:** $App^{NL\text{-}G\text{-}F}$ mice (20 homozygous and 21 heterogeneous) and 12 age-matched wild-type mice were investigated longitudinally from 2.5 to 10 mo of age with ^{18}F-florbetaben Aβ PET and ^{18}F-GE-180 18-kDa translocator protein (TSPO) PET. Voxelwise analysis of SUV ratio images was performed using statistical parametric mapping. All mice underwent a Morris water maze test of spatial learning after their final scan. Quantification of fibrillar Aβ and activated microglia by immunohistochemistry and biochemistry served for validation of the PET results. **Results:** The periaqueductal gray emerged as a suitable pseudo reference tissue for both tracers. Homozygous $App^{NL\text{-}G\text{-}F}$ mice had a rising SUV ratio in cortex and hippocampus for Aβ (+9.1%, +3.8%) and TSPO (+19.8%, +14.2%) PET from 2.5 to 10 mo of age (all $P < 0.05$), whereas heterozygous $App^{NL\text{-}G\text{-}F}$ mice did not show significant changes with age. Significant voxelwise clusters of Aβ deposition and microglial activation in homozygous mice appeared at 5 mo of age. Immunohistochemical and biochemical findings correlated strongly with the PET data. Water maze escape latency was significantly elevated in homozygous $App^{NL\text{-}G\text{-}F}$ mice compared with wild-type at 10 mo of age and was associated with high TSPO binding. **Conclusion:** Longitudinal PET in $App^{NL\text{-}G\text{-}F}$ knock-in mice enables monitoring of amyloidogenesis and neuroinflammation in homozygous mice but is insensitive to minor changes in heterozygous animals. The combination of PET with behavioral tasks in $App^{NL\text{-}G\text{-}F}$ treatment trials is poised to provide important insights in preclinical drug development.

Received Feb. 12, 2019; revision accepted May 15, 2019.
For correspondence or reprints contact: Matthias Brendel, Department of Nuclear Medicine, LMU Munich, Marchioninistrasse 15, Munich 81377 Germany.
E-mail: matthias.brendel@med.uni-muenchen.de
*Contributed equally to this work.
Published online Jul. 13, 2019.

Key Words: Alzheimer disease; β-amyloid; microglia; $App^{NL\text{-}G\text{-}F}$; spatial learning

J Nucl Med 2019; 60:1787–1793
DOI: 10.2967/jnumed.119.227322

Alzheimer disease (AD) is the most common neurodegenerative disease, with an incidence that increases exponentially with age, such that the prevalence exceeds 10% among octogenarians and 30% for nonagenarians. This epidemic is placing a growing socioeconomic burden on health care in societies with aging populations (*1*). The neuropathology of AD classically includes the accumulation of amyloid-β peptide (Aβ) as extracellular plaques, and fibrillary tau aggregates within neurons. Activation of multiple neuroinflammatory pathways mediated by activated microglia expressing high levels of the marker 18-kDa translocator protein (TSPO) completes the triad of markers. These pathologic conditions, restricted mainly to the cerebral cortex and the hippocampus, lead to a progressive decline in cognitive function, usually first manifesting as memory complaints (*2–6*). The identification of familial AD mutations in the amyloid precursor protein (APP) gene has led to the generation of several transgenic mouse models that overexpress APP (*7,8*). These first-generation mouse models exhibit AD pathology, but the nonphysiologic overexpression of APP may cause additional phenotypes unrelated to AD. To circumvent these intrinsic drawbacks, second-generation APP knock-in mice that carry pathogenic mutations in the APP gene have been established (*9*). For example, $App^{NL\text{-}G\text{-}F}$ mice carry a mutant APP gene encoding the humanized Aβ sequence (G601R, F606Y, and R609H) with 3 pathogenic mutations, namely Swedish (KM595/596NL), Beyreuther/Iberian (I641F), and Arctic (E618G). Homozygotic $App^{NL\text{-}G\text{-}F}$ mice progressively exhibit widespread Aβ accumulation along with activation of microglia and astrocytes from 2 mo of age and express behavioral symptoms in the form of declining spatial learning ability from 8 to 12 mo of age (*10–13*). Given their physiologic expression of APP in comparison to transgenic mouse models, these knock-in mice are not characterized by massively elevated expression of the intracellular domain of APP or soluble APPα (*9*). Therefore, this mouse model potentially

avoids confounds due to nonphysiologic signaling in therapy testing trials.

Previous studies have shown that small-animal PET is a suitable noninvasive tool for monitoring of therapeutic trials targeting AD pathology (*14,15*). We previously established small-animal PET for monitoring of Aβ deposition and microglial activation in APP-overexpressing mice, yielding excellent correlations with histologic and biochemical assessments (*16*). Given this background, the aim of this study was to transfer small-animal PET methodology to the $App^{NL\text{-}G\text{-}F}$ mouse model in a longitudinal investigation of the amyloid tracer ^{18}F-florbetaben and the TSPO tracer ^{18}F-GE-180. We confirmed the new dual-tracer PET results relative to findings obtained by immunohistochemistry and biochemistry and correlated the neuropathology findings with scores in a test of spatial learning.

MATERIALS AND METHODS

Animals and Study Design

All experiments were performed in compliance with the National Guidelines for Animal Protection, Germany, with the approval of the regional animal committee (Regierung Oberbayern) and were overseen by a veterinarian. Animals were housed in a temperature- and humidity-controlled environment with a 12-h light–dark cycle and free access to food (Sniff; Soest) and water. The experiments were performed in mixed-sex groups of heterozygous (n = 21) and homozygous (n = 20) $App^{NL\text{-}G\text{-}F}$ mice, which is a knock-in mouse line generated by Saito et al. (*11*), and a group of age-matched wild-type mice. Small-animal PET examinations (Aβ and TSPO) were performed in a longitudinal design at baseline (2.5 mo of age) and 3 follow-up measurements (5.0, 7.5, and 10.0 mo). Serial scans of both tracers deriving from a total of 12 age- and sex-matched wild-type mice served as controls, in consideration of the age-dependent increase of cortical TSPO PET signal in wild-type mice (*17*). All available mice underwent Morris water maze tests within 2 wk after their scan. After behavioral testing, the mice were deeply anesthetized before transcardial perfusion and brain extraction. A minimum of 4 brains per genotype were processed for immunohistochemistry and biochemistry in randomly selected hemispheres.

PET Imaging

PET Data Acquisition, Reconstruction, and Postprocessing. For all PET procedures, we used an established standardized protocol for radiochemistry, acquisition, and preprocessing (*16*). In brief, ^{18}F-GE-180 TSPO small-animal PET (13.4 ± 1.6 MBq; ~400–1,400 GBq/μmol) recordings with an emission window of 60–90 min after injection were obtained to measure cerebral TSPO expression, along with ^{18}F-florbetaben Aβ-small-animal PET (12.9 ± 1.7 MBq; ~30–80 GBq/μmol) recordings with an emission window of 30–60 min after injection for assessment of fibrillar cerebral amyloidosis. Two $App^{NL\text{-}G\text{-}F}$ mice aged 11 mo were imaged in a dynamic setting (^{18}F-florbetaben: 0–60 min after injection; ^{18}F-GE-180: 0–90 min after injection) and their results compared with historic dynamic wild-type data for validation of the previously established time windows in this model. Anesthesia was maintained from just before tracer injection to the end of the imaging time window.

PET Image Analysis. We performed all analyses using PMOD (version 3.5; PMOD technologies). First, intensity normalization of images to SUV images was conducted by the previously validated myocardium correction method (*18*) for TSPO PET and by conventional SUV calculation for Aβ PET. Voxel-based comparisons of SUV images between $App^{NL\text{-}G\text{-}F}$ (n = 13 per tracer, 10 mo) and wild-type mice (n = 6 per tracer, 10 mo) were performed to investigate a suitable pseudo reference tissue for PET quantification in the $App^{NL\text{-}G\text{-}F}$ mouse model. The judgment of suitability was also informed by the immunohistochemistry results described below. A suitable pseudo reference tissue was defined as a brain region lacking any genotypic difference in PET and immunohistochemistry results for both radioligands. These criteria led us to select the mesencephalic periaqueductal gray (PAG, comprising 20 mm^3) as a pseudo reference region for calculation of SUV ratio (SUVR) for both Aβ and TSPO PET (Fig. 1). Two bilateral frontal cortical target volumes of interest (VOIs, comprising 24 mm^3 each) and 2 bilateral hippocampal target VOIs (comprising 10 mm^3 each) were used for both tracers. Target–to–reference-tissue SUVRs were calculated for cortex ($SUVR_{CTX/PAG}$) and hippocampus ($SUVR_{HIP/PAG}$) for Aβ and TSPO PET.

SPM Analysis. For both tracers, whole-brain voxelwise comparisons of PAG-scaled SUVR images between groups of knock-in and wild-type mice were performed as described previously (*19,20*).

Behavioral Testing

Mice (homozygous $App^{NL\text{-}G\text{-}F}$: n = 11, heterozygous $App^{NL\text{-}G\text{-}F}$: n = 14, wild-type: n = 3) underwent a Morris water maze test for spatial learning and memory deficits, which was performed according to a standard protocol with small adjustments (*21*). The video tracking software EthoVision XT (Noldus) was used for analyses of escape latency during the training period and during the probe trial.

Immunohistochemistry and Biochemistry

In brain regions corresponding to PET VOIs (Supplemental Table 1; supplemental materials are available at http://jnm.snmjournals.org), histochemistry was performed for fibrillar Aβ (methoxy-X04; Tocris) and immunohistochemistry for activated microglia using an Iba1 primary antibody (Wako) as previously established (*17,22*). NAB228 (Santa Cruz) was used for immunohistochemistry labeling of fibrillar

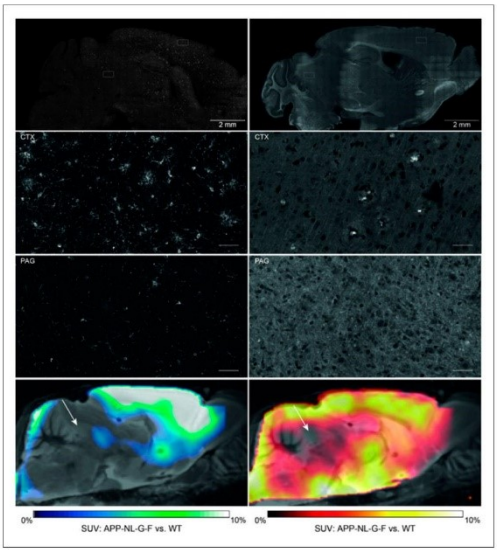

FIGURE 1. Immunohistochemistry reveals lowest microglial activation (left, Iba-1) and amyloid deposition (right, methoxy-X04) in PAG of $App^{NL\text{-}G\text{-}F}$ mice aged 10 mo (overview and zoom in upper 3 panels). Suitability of PAG (white arrows) as pseudo reference tissue was further assessed by comparing SUV of TSPO- and Aβ PET images between genotypes (overview in lowest panel). WT = wild-type.

and nonfibrillar Aβ depositions. Hemispheres from 5 homozygous $App^{NL\text{-}G\text{-}F}$, 5 heterozygous $App^{NL\text{-}G\text{-}F}$, and 4 wild-type mice were used for immunohistochemistry. Assessment of Aβ40 and Aβ42 was performed as previously described (*23*). Biochemical analyses were performed in samples from the entire forebrain. Soluble Trem2 protein was extracted from brain tissue with Tris-buffered saline, and measured by ELISA, using polyclonal sheep antibody for coating (AF1729; R&D Systems) and biotinylated polyclonal sheep antibody (BAF1729; R&D Systems) together with streptavidin-horseradish peroxidase (N-100; ThermoFisher Scientific) for detection. Hemispheres from 8 homozygous $App^{NL\text{-}G\text{-}F}$, 14 heterozygous $App^{NL\text{-}G\text{-}F}$, and 4 wild-type mice were used for biochemical analyses.

Statistics

Group comparisons of VOI-based PET results between knock-in and wild-type mice were performed by 1-way ANOVA and Tukey post hoc tests for multiple comparisons, calculated by SPSS 25 Statistics (IBM). Two-sided *t* tests were used to compare terminal multimodal readouts of homozygous $App^{NL\text{-}G\text{-}F}$ with wild-type or heterozygous $App^{NL\text{-}G\text{-}F}$ groups. Two-way ANOVA was applied to assess methoxy-X04 and NAB228 fluorescence intensity changes distant and close to plaques. For correlation analyses in $App^{NL\text{-}G\text{-}F}$, Pearson coefficients of correlation (*R*) were calculated for normally distributed readouts after Kolmogorov–Smirnov testing for normalcy. For non-normally distributed readouts, Spearman coefficients of correlation (r_S) were calculated. A threshold *P* value of less than 0.05 was considered significant for rejection of the null hypothesis. Sample size calculations for potential upcoming treatment trials were performed for longitudinal (2.5–10.0 mo) and terminal measures in the cortical VOI for both ligands in homozygous $App^{NL\text{-}G\text{-}F}$ mice. We used a simplified *t*-statistic model with assumptions of a type I error α of 0.05, a power of 0.8, and a treatment effect of 50% calculated in G*Power (version 3.1; Heinrich-Heine University). For the power calculation, we simulated the treatment group by calculating longitudinal differences within single $App^{NL\text{-}G\text{-}F}$ mice and terminal differences of single $App^{NL\text{-}G\text{-}F}$ mice by multiplying the mean endpoint of wild-type for each tracer by 0.5, corresponding to the 50% treatment effect.

RESULTS

Pseudo Reference Region

Immunohistochemistry revealed a widespread amyloidosis and microglial activation in $App^{NL\text{-}G\text{-}F}$ mice at 10 mo of age, involving most regions of the forebrain (Fig. 1). Regions with relatively low amyloidosis and microglial activation were observed in parts of the hindbrain, that is, vermis, midbrain, and notably the PAG. SUV differences between genotypes at 10 mo of age fitted to immunohistochemistry and revealed the lowest ^{18}F-florbetaben and ^{18}F-GE180 alterations in the hindbrain (Fig. 1). SUV analysis at the final time point revealed that an oval VOI primarily comprising PAG voxels yields a suitable pseudo reference region (^{18}F-florbetaben SUV: $App^{NL\text{-}G\text{-}F}$, 0.47 ± 0.08; wild-type, 0.46 ± 0.09 [not statistically significant]/^{18}F-GE180 SUV with myocardium correction (*18*): $App^{NL\text{-}G\text{-}F}$, 0.22 ± 0.02; wild-type, 0.23 ± 0.02 [not statistically significant]). $SUVR_{CTX/PAG}$ time–activity-curves of aged $App^{NL\text{-}G\text{-}F}$ mice revealed stable uptake differences for 30–60 min after injection for ^{18}F-florbetaben and 60–90 min after injection for ^{18}F-GE180 imaging when compared with historic wild-type data (Supplemental Fig. 1). Furthermore, the comparison of methoxy-X04 and NAB228 staining revealed only a minor fraction of fibrillar Aβ in amyloid plaques in the entire brain (Fig. 2), which predicted a relatively lower ^{18}F-florbetaben signal than in the historically investigated amyloid mouse models.

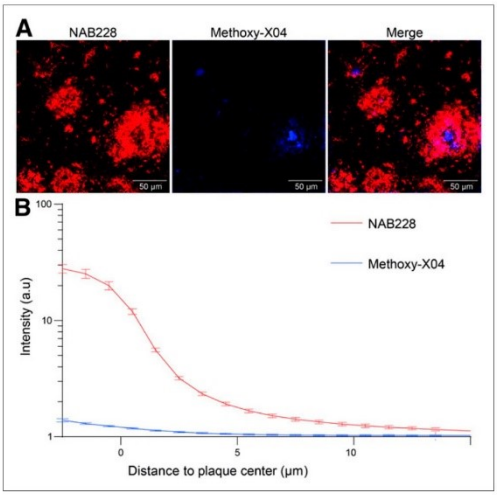

FIGURE 2. (A) Minor dense fraction of cortical Aβ plaques in $App^{NL\text{-}G\text{-}F}$ mice as assessed by NAB228 (red) and methoxy-X04 (blue) costaining. (B) Graph indicates mean methoxy-X04 and NAB228 fluorescence intensity profiles from plaque border; 2-way ANOVA interaction staining × distance, $F_{43,704} = 14.79$, $P < 0.001$. Data are presented as mean ± SEM with 9 mice per group. Minimal plaque number analyzed per mouse is 41. ***$P < 0.001$. a.u = arbitrary units.

Dual-Tracer PET Analyses

A comprehensive overview of the PET results is provided in Table 1. The age dependence of the retention of the 2 tracers is presented in Figure 3 and illustrated in Supplemental Figure 2.

Aβ PET Findings. Homozygous $App^{NL\text{-}G\text{-}F}$ mice already showed elevated cortical ^{18}F-florbetaben SUVR compared with their baseline as early as 5 mo of age (+3.4%; $P < 0.05$), which increased further at 10 mo (+9.1%; $P < 0.001$). Hippocampal increases in SUVR first became apparent at 7.5 mo (+2.6%; $P < 0.05$) and were more conspicuous at 10 mo (+3.8%; $P < 0.001$). Required sample sizes for detection of a 50% Aβ PET treatment effect in the cortex of homozygous $App^{NL\text{-}G\text{-}F}$ mice were $n = 11$ for evaluation of longitudinal measures between 2.5 and 10 mo and $n = 8$ for the terminal time point. The heterozygous genotype did not show significant changes in ^{18}F-florbetaben SUVR relative to baseline at any age.

TSPO PET Findings. Homozygous $App^{NL\text{-}G\text{-}F}$ mice revealed the first evidence of increased cortical ^{18}F-GE-180 uptake compared with baseline as early as 5 mo (+6.5%; $P < 0.05$), which increased strongly by 10 mo (+19.8%; $P < 0.001$). Significantly elevated ^{18}F-GE-180 SUVR in the hippocampus was present at 7.5 mo (+10.8%; $P < 0.001$), which increased further by 10 mo (+14.2%; $P < 0.001$). Required sample sizes for detection of a 50% TSPO PET treatment effect in the cortex of homozygous $App^{NL\text{-}G\text{-}F}$ mice were $n = 16$ for evaluation of longitudinal measures between 2.5 and 10 mo and $n = 11$ for the terminal time point. The heterozygous genotype revealed neither cortical nor hippocampal microglial activation at any age.

Correlation Analyses. Significant positive associations between Aβ and TSPO PET quantification were observed for the cortex ($R = 0.64$; $P < 0.001$; Fig. 3C) and the hippocampus ($R = 0.48$; $P < 0.05$; Fig. 3F).

TABLE 1
Overview of Small-Animal PET Results

		Amyloid PET				TSPO PET			
				SUVR				SUVR	
Group	Age (mo)	*n*	Sex	Cortex	Hippocampus	*n*	Sex	Cortex	Hippocampus
Homozygous App^{NL-G-F}	2.5	20	9♂/11♀	0.86 ± 0.02	0.95 ± 0.01	18	9♂/9♀	0.79 ± 0.05	0.82 ± 0.04
	5.0	17	6♂/11♀	0.89 ± 0.03*	0.96 ± 0.02	17	6♂/11♀	0.84 ± 0.04*	0.86 ± 0.03
	7.5	13	6♂/7♀	0.92 ± 0.05†	0.97 ± 0.03*	14	6♂/8♀	0.91 ± 0.04†	0.91 ± 0.06†
	10.0	13	6♂/7♀	0.94 ± 0.03†	0.98 ± 0.02†	13	6♂/7♀	0.94 ± 0.06†	0.94 ± 0.07†
Heterozygous App^{NL-G-F}	2.5	21	13♂/8♀	0.87 ± 0.03	0.95 ± 0.03	20	12♂/8♀	0.78 ± 0.06	0.81 ± 0.04
	5.0	20	12♂/8♀	0.87 ± 0.04	0.94 ± 0.02	20	12♂/8♀	0.78 ± 0.05	0.81 ± 0.04
	7.5	15	9♂/6♀	0.89 ± 0.04	0.95 ± 0.02	17	10♂/7♀	0.77 ± 0.04	0.81 ± 0.05
	10.0	13	8♂/5♀	0.89 ± 0.04	0.95 ± 0.03	13	8♂/5♀	0.79 ± 0.04	0.81 ± 0.05
Wild-type C57BL/6	2.5	6	3♂/3♀	0.87 ± 0.03	0.96 ± 0.01	6	3♂/3♀	0.75 ± 0.07	0.80 ± 0.04
	10.0	6	3♂/3♀	0.86 ± 0.01	0.95 ± 0.01	6	3♂/3♀	0.82 ± 0.04	0.84 ± 0.03

*$P < 0.05$ (1-way ANOVA including post hoc Tukey testing vs. baseline).
†$P < 0.001$ (1-way ANOVA including post hoc Tukey testing vs. baseline).
Numbers (*n*) of mice included in PET analyses by sex are provided for each tracer and age.

Voxelwise Analyses. Voxelwise group contrasts between knock-in and wild-type animals are shown in Supplemental Figure 3. By this exploratory approach, the strongest differences in ^{18}F-florbetaben uptake between homozygous *App*$^{NL-G-F}$ and wild-type mice ($P < 0.001$, uncorrected) were discerned in the left thalamus. This first became apparent at 5 mo, whereas comparable thalamic

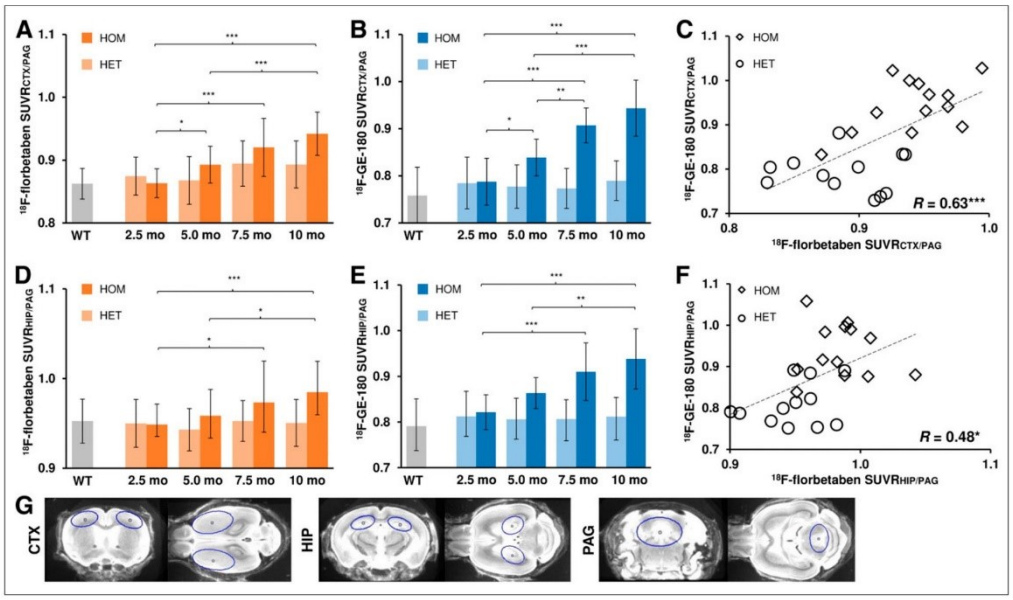

FIGURE 3. (A, B, D, and E) Age dependence of Aβ and TSPO radiotracer uptake in frontal cortex and hippocampus of homozygous (HOM) and heterozygous (HET) *App*$^{NL-G-F}$ mice. Group comparisons of VOI-based small-animal PET results between knock-in mouse groups were assessed by 1-way ANOVA and Tukey post hoc test. (C and F) Correlation between Aβ deposition and microglial activation in frontal cortex and in hippocampus measured by dual-tracer small-animal PET (*R* indicates Pearson coefficients of correlation). (G) Definitions of cortical (CTX), hippocampal (HIP), and PAG VOIs in coronal and axial slices on MRI mouse brain atlas. *$P < 0.05$. **$P < 0.01$. ***$P < 0.001$. WT = wild-type.

elevations in the heterozygous genotype emerged only at 7.5 mo. Significant SUVR increases in neocortical areas were observed in homozygous $App^{NL\text{-}G\text{-}F}$ mice only at 10 mo of age, when 29% of the total brain volume had elevated ^{18}F-florbetaben signal relative to the wild-type group.

Voxelwise TSPO PET analysis revealed microglial activation in homozygous $App^{NL\text{-}G\text{-}F}$ mice in the frontal cortex and the hippocampus starting at 5 mo (18% of total brain volume, $P < 0.001$, uncorrected), which increased to involvement of 48% of total brain volume at 10 mo of age ($P < 0.001$, uncorrected), including thalamic regions. Heterozygous $App^{NL\text{-}G\text{-}F}$ animals showed no differences in ^{18}F-GE-180 uptake relative to wild-type at any age.

Correlation with Multimodal Terminal Readouts

Average values for the different genotypes of all terminal readouts at the age of 10 mo are presented in Supplemental Table 1. We observed strong increases in all biochemical (Aβ40, Aβ42, sTrem2) and (immuno)histochemistry (Iba1, methoxy-X04; Supplemental Fig. 4) readouts in the comparison of homozygous $App^{NL\text{-}G\text{-}F}$ with wild-type or heterozygous $App^{NL\text{-}G\text{-}F}$ animals. Spatial learning score was substantially impaired in the homozygous $App^{NL\text{-}G\text{-}F}$ compared with wild-type groups (latency to platform, +2.1-fold, $P < 0.05$, 2-tailed), with no such difference for heterozygous $App^{NL\text{-}G\text{-}F}$. All correlations between SUVRs at 10 mo of age and multimodal terminal readouts are illustrated in Figure 4.

Biochemistry. Aβ42 concentration correlated highly with cortical ^{18}F-florbetaben ($r_S = 0.69$; $P < 0.001$) and ^{18}F-GE-180 uptake ($r_S = 0.70$; $P < 0.001$). Furthermore, significant Aβ42 correlations with hippocampal SUVRs were observed for both tracers ($P < 0.01$). Quantification of sTrem2 correlated with the cortical ($r_S = 0.61$; $P < 0.01$) and hippocampal ($r_S = 0.53$; $P < 0.05$) SUVR of ^{18}F-GE-180.

Immunohistochemistry. Hippocampal ($r_S = 0.90$; $P < 0.001$) and cortical ($R = 0.75$; $P < 0.05$) ^{18}F-florbetaben uptake strongly correlated with plaque burden, measured by methoxy-X04 histology in the corresponding regions. The Iba1 burden, which is indicative of activated microglia, correlated with uptake of the TSPO tracer ^{18}F-GE-180 in neocortex ($R = 0.92$; $P < 0.001$) and hippocampus ($R = 0.78$; $P < 0.01$).

Behavioral Analysis. There was a moderate significant association between cortical ^{18}F-GE-180 SUVR and escape latency at 10 mo ($R = 0.41$; $P < 0.05$), meaning that mice with stronger microglial activation needed significantly more time to reach the platform in the Morris water maze test.

DISCUSSION

To our knowledge, this was the first longitudinal dual-tracer PET study of cerebral amyloidosis and neuroinflammation in a knock-in AD mouse model. After modification of standardized PET protocols to circumvent model-specific difficulties in homozygous $App^{NL\text{-}G\text{-}F}$ knock-in mice, we detected strong progressive increases of ^{18}F-florbetaben and ^{18}F-GE-180 uptake with age. Terminal validation analyses by immunohistochemistry and biochemistry confirmed these in vivo PET results. The present findings establish the basis for serial PET monitoring of therapeutic agents targeting Aβ deposition and microglial activation in $App^{NL\text{-}G\text{-}F}$ mice.

Two model-specific issues were encountered and solved for establishing PET imaging in $App^{NL\text{-}G\text{-}F}$ mice: first, the widespread amyloid pathology in the brain hampered the use of previously established reference regions such as the cerebellum or white matter (*16*). SUVR scaling by an appropriate intracerebral reference tissue represents an important tool to generate robust PET results during short acquisitions in mice. This is crucial for the

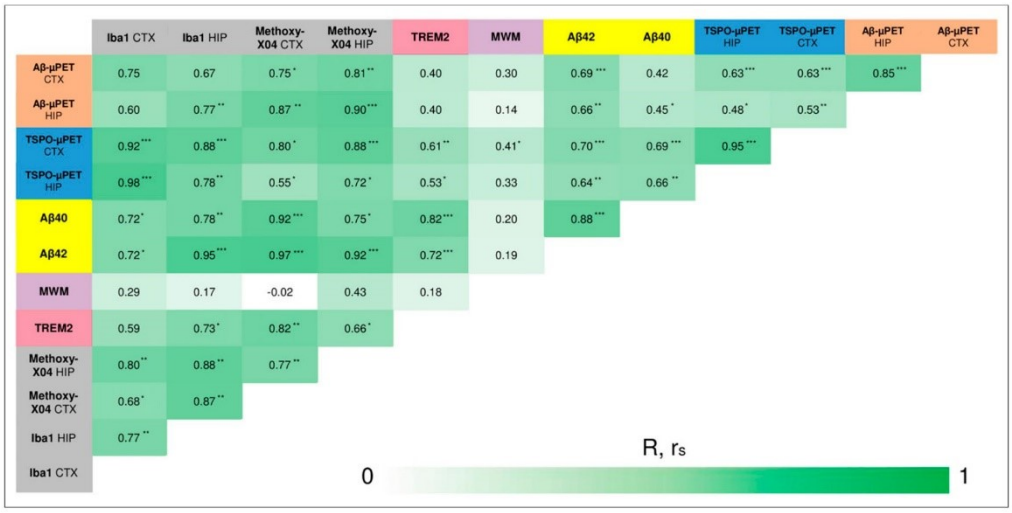

FIGURE 4. Correlation analyses of all terminal readouts. Pearson coefficients of correlation (R) were calculated for normally distributed readouts (small-animal PET, behavior, Iba1, methoxy-X04). For remaining not normally distributed readouts, Spearman coefficients of correlation (r_S) were calculated. *$P < 0.05$. **$P < 0.01$. ***$P < 0.001$. CTX = cortex; HIP = hippocampal; MWM = Morris Water Maze; TREM2 = Triggering receptor expressed on myeloid cells 2.

present $App^{NL\text{-}G\text{-}F}$ model mice, which are vulnerable to more stress-related drop-outs than are other amyloid mouse models (*10*). Although full kinetic modeling with arterial blood sampling represents the gold standard for small-animal PET quantification, that approach is hardly feasible in mouse studies encompassing up to 4 pairs of PET sessions. Therefore, we used a variance analysis for both PET tracers together with immunohistochemistry assessment to identify the most valid pseudo reference tissue, which proved to be PAG of the mesencephalon. Validation in serial dual PET imaging revealed robust quantification of SUVR relative to PAG, and terminal assessments substantiated our use of this pseudo reference tissue through the excellent correlation of terminal PET results with immunohistochemistry gold standards. A low dropout rate during serial PET imaging (<10% per time point) also encourages the use of our newly established SUVR protocol. We note that the SUVR range fell below unity for quantification of both tracers, because of higher unspecific binding in the PAG reference tissue than in cortical or hippocampal target regions. Using the reference tissue normalization but reducing variance in the population stabilized PET quantification, just as in our previous investigations of both ligands (*16,24*).

Another aspect of the present model concerns the fraction of dense fibrillar Aβ in the plaques of $App^{NL\text{-}G\text{-}F}$ mice, which is lower than in other transgenic amyloid mouse models. This is an important technicality, as fluorinated Aβ PET tracers such as ^{18}F-florbetaben have high affinity for dense fibrillary plaques but exhibit only low binding in diffuse plaques (*25*). As expected from this fact, we observed a lesser longitudinal increase for ^{18}F-florbetaben binding than for ^{18}F-GE-180 from the plaque onset until the full-blown pathology occurring at 10 mo of age (9.1% vs. 19.8%). In contrast, we had earlier found similar increases of the same 2 radioligands in APP-SL70 (18.3% vs. 17.6%) (*26*) and PS2APP mice (+19.8% vs. +20.2%) (*16*). Thus, whereas quantitative Aβ imaging to ^{18}F-florbetaben PET is feasible in $App^{NL\text{-}G\text{-}F}$ mice, the tracer misses at least half of the true plaque burden, which constitutes a weakness of using this particular radioligand in the knock-in mouse model. This property needs to be addressed in future studies of Aβ-targeting therapies or genetic modifications with differential effects on the expressions of dense and diffuse parts of the plaque (*27*).

Voxelwise group contrasts between knock-in and wild-type animals revealed increased ^{18}F-florbetaben uptake in homozygous $App^{NL\text{-}G\text{-}F}$ mice already at 5 mo of age. Notably, early increases in amyloid binding were present in the thalamus of homozygous and heterozygous $App^{NL\text{-}G\text{-}F}$ animals. This finding in the thalamus of knock-in mice is in contrast to sporadic AD, and the thalamus is not typically considered a target region for therapy studies in AD mouse models.

Serial PET analyses and terminal assessments of our study indicated parallel increases of amyloidosis and microglial activation with age in the transgenic knock-in mice. The observed strong correlations between cortical TSPO and Aβ readouts were expected from the results of a published study, which demonstrated a link between amyloidosis and neuroinflammation based on comparative profiling of cortical gene expression in AD patients and in the $App^{NL\text{-}G\text{-}F}$ mouse model (*13*). Our recent study of PS2APP mice showed that the concentration of sTrem2, which is expressed by microglia as a mediator of phagocytic clearance of debris (*6*), strongly correlates with TSPO and Aβ PET signals (*28*). The present biochemical analysis of sTrem2 also showed strong correlations with terminal TSPO PET but not with Aβ PET. This finding may indicate that sTrem2 serves as a valid biomarker for microglial activation in $App^{NL\text{-}G\text{-}F}$ mice but that its expression is not so tightly coupled to fibrillar Aβ levels in $App^{NL\text{-}G\text{-}F}$ mice as in PS2APP mice.

Recent publications report that homozygous $App^{NL\text{-}G\text{-}F}$ mice show a subtle, progressive deterioration in performance of spatial learning trials, deficits in flexible learning, and reduced attentional performance compared with wild-type (*10*). Consistent with these findings, we observed a significant deficit in spatial learning in homozygous $App^{NL\text{-}G\text{-}F}$ mice in performing the hippocampus-related Morris water maze test. However, the learning and memory deficits in $App^{NL\text{-}G\text{-}F}$ mice should be further investigated since another study has reported intact learning and memory in homozygous $App^{NL\text{-}G\text{-}F}$ mice at the age of as much as 15–18 mo (*12*). Spatial learning performance at 10 mo of age did not correlate with longitudinal Aβ PET or with terminal immunohistochemistry or biochemical measures of amyloidosis, as is in line with a recent review of different transgenic mouse models of AD (*29*). Our previous study with TSPO PET in PS2APP revealed some evidence for an association between consistently strong early and terminal neuroinflammation with a better preservation of cognitive function (*30*), suggesting a net protective effect of microglial activation. In contrast, the deterioration in spatial learning in aged $App^{NL\text{-}G\text{-}F}$ mice correlated significantly with increased cortical TSPO PET SUVR at the terminal time point. With regard to the specific plaque composition observed in $App^{NL\text{-}G\text{-}F}$, which has less dense but more diffuse plaques than the first-generation amyloid mouse models, the present findings call for further examination of the specific role of microglial activation in $App^{NL\text{-}G\text{-}F}$ neuropathology. Furthermore, we should in future consider applying other behavioral assessments in addition to the Morris water maze test of spatial learning. Intermouse-model comparisons of findings from imaging in conjunction with other biomarkers are summarized in Supplemental Table 2.

Molecular imaging with PET uniquely affords longitudinal monitoring of disease-related alterations and interventions in individual animals and can allow prediction of progression and therapeutic effects from early baseline characteristics (*14,15*). Recent therapeutic studies on transgenic mouse models monitored by PET, such as using an inhibitor of the β-site APP-cleaving enzyme 1, have already shown encouraging results with respect to delayed pathology (*14,31,32*). Our serial in vivo PET results together with ex vivo observations in $App^{NL\text{-}G\text{-}F}$ mice, representing an aggressively neurotoxic knock-in amyloid model with cognitive impairment, support the use of these methods for interventional studies, especially when fibrillary parts of the plaque are targeted by the therapy, as is especially relevant for antiamyloid antibodies.

CONCLUSION

Analysis of Aβ and TSPO PET imaging in $App^{NL\text{-}G\text{-}F}$ mice is complicated by the widespread cerebral pathology and relatively low fibrillarity of Aβ plaques but is feasible using PAG as a pseudo reference region. Progression of neuropathology can be tracked by serial ^{18}F-florbetaben and ^{18}F-GE-180 PET in homozygous $App^{NL\text{-}G\text{-}F}$ mice, whereas heterozygous $App^{NL\text{-}G\text{-}F}$ animals present only minor changes to these methods. The combination of PET with a test of cognition in this new knock-in AD model, $App^{NL\text{-}G\text{-}F}$, is a promising test-bed for preclinical drug development.

DISCLOSURE

Florbetaben precursor was provided by Life Molecular. GE Healthcare made GE-180 cassettes available through an early-access

model. Seed funding was provided by Verein zur Förderung von Wissenschaft und Forschung an der Medizinischen Fakultät der Ludwig-Maximilians-Universität München. This work was supported by the Deutsche Forschungsgemeinschaft (DFG) by a grant to Matthias Brendel and Axel Rominger (BR4580/1-1 and RO5194/1-1) and within the framework of the Munich Cluster for Systems Neurology (EXC1010SyNergy). Peter Bartenstein and Axel Rominger received speaking honoraria from Life Molecular; Irena Brzak and Ulf Neumann are employees of Novartis. No other potential conflict of interest relevant to this article was reported.

ACKNOWLEDGMENTS

We thank Karin Bormann-Giglmaier for excellent technical assistance. We acknowledge Inglewood Biomedical Editing for manuscript editing.

KEY POINTS

QUESTION: Is it possible to monitor preclinical trials using APP knock-in mice by means of small-animal PET for Aβ and 18 kDa TSPO?

PERTINENT FINDINGS: This longitudinal preclinical investigation revealed progressively increasing uptake of PET tracers for Aβ and 18 kDa TSPO in APP knock-in mice. Terminal PET findings were highly correlated with ex vivo gold standard assessments.

IMPLICATIONS FOR PATIENT CARE: PET in APP knock-in mice present a new instrument for bench to bedside therapy monitoring without interference from APP overexpression.

REFERENCES

1. Ziegler-Graham K, Brookmeyer R, Johnson E, Arrighi HM. Worldwide variation in the doubling time of Alzheimer's disease incidence rates. *Alzheimers Dement.* 2008;4:316–323.
2. Braak H, Braak E. Demonstration of amyloid deposits and neurofibrillary changes in whole brain sections. *Brain Pathol.* 1991;1:213–216.
3. Hyman BT, Phelps CH, Beach TG, et al. National Institute on Aging–Alzheimer's Association guidelines for the neuropathologic assessment of Alzheimer's disease. *Alzheimers Dement.* 2012;8:1–13.
4. Serrano-Pozo A, Frosch MP, Masliah E, Hyman BT. Neuropathological alterations in Alzheimer disease. *Cold Spring Harb Perspect Med.* 2011;1:a006189.
5. Querfurth HW, LaFerla FM. Alzheimer's disease. *N Engl J Med.* 2010;362:329–344.
6. Heneka MT, Carson MJ, Khoury JE, et al. Neuroinflammation in Alzheimer's disease. *Lancet Neurol.* 2015;14:388–405.
7. Jonsson T, Atwal JK, Steinberg S, et al. A mutation in APP protects against Alzheimer's disease and age-related cognitive decline. *Nature.* 2012;488:96–99.
8. Hsiao K, Chapman P, Nilsen S, et al. Correlative memory deficits, Aβ elevation, and amyloid plaques in transgenic mice. *Science.* 1996;274:99–102.
9. Sasaguri H, Nilsson P, Hashimoto S, et al. APP mouse models for Alzheimer's disease preclinical studies. *EMBO J.* 2017;36:2473–2487.
10. Masuda A, Kobayashi Y, Kogo N, Saito T, Saido TC, Itohara S. Cognitive deficits in single App knock-in mouse models. *Neurobiol Learn Mem.* 2016;135:73–82.
11. Saito T, Matsuba Y, Mihira N, et al. Single App knock-in mouse models of Alzheimer's disease. *Nat Neurosci.* 2014;17:661–663.
12. Sakakibara Y, Sekiya M, Saito T, Saido TC, Iijima KM. Cognitive and emotional alterations in App knock-in mouse models of Aβ amyloidosis. *BMC Neurosci.* 2018;19:46.
13. Castillo E, Leon J, Mazzei G, et al. Comparative profiling of cortical gene expression in Alzheimer's disease patients and mouse models demonstrates a link between amyloidosis and neuroinflammation. *Sci Rep.* 2017;7:17762.
14. Brendel M, Jaworska A, Overhoff F, et al. Efficacy of chronic BACE1 inhibition in PS2APP mice depends on the regional Aβ deposition rate and plaque burden at treatment initiation. *Theranostics.* 2018;8:4957–4968.
15. Brendel M, Jaworska A, Herms J, et al. Amyloid-PET predicts inhibition of de novo plaque formation upon chronic γ-secretase modulator treatment. *Mol Psychiatry.* 2015;20:1179–1187.
16. Brendel M, Probst F, Jaworska A, et al. Glial activation and glucose metabolism in a transgenic amyloid mouse model: a triple-tracer PET study. *J Nucl Med.* 2016;57:954–960.
17. Brendel M, Focke C, Blume T, et al. Time courses of cortical glucose metabolism and microglial activity across the life span of wild-type mice: a PET study. *J Nucl Med.* 2017;58:1984–1990.
18. Deussing M, Blume T, Vomacka L, et al. Coupling between physiological TSPO expression in brain and myocardium allows stabilization of late-phase cerebral [^{18}F]GE180 PET quantification. *Neuroimage.* 2018;165:83–91.
19. Rominger A, Brendel M, Burgold S, et al. Longitudinal assessment of cerebral b-amyloid deposition in mice overexpressing Swedish mutant b-amyloid precursor protein using ^{18}F-florbetaben PET. *J Nucl Med.* 2013;54:1127–1134.
20. Sawiak SJ, Wood NI, Williams GB, Morton AJ, Carpenter TA. Voxel-based morphometry in the R6/2 transgenic mouse reveals differences between genotypes not seen with manual 2D morphometry. *Neurobiol Dis.* 2009;33:20–27.
21. Bromley-Brits K, Deng Y, Song W. Morris water maze test for learning and memory deficits in Alzheimer's disease model mice. *J Vis Exp.* 2011;53:e2920
22. Dorostkar MM, Dreosti E, Odermatt B, Lagnado L. Computational processing of optical measurements of neuronal and synaptic activity in networks. *J Neurosci Methods.* 2010;188:141–150.
23. Neumann U, Rueeger H, Machauer R, et al. A novel BACE inhibitor NB-360 shows a superior pharmacological profile and robust reduction of amyloid-beta and neuroinflammation in APP transgenic mice. *Mol Neurodegener.* 2015;10:44.
24. Overhoff F, Brendel M, Jaworska A, et al. Automated spatial brain normalization and hindbrain white matter reference tissue give improved [^{18}F]-florbetaben PET quantitation in Alzheimer's model mice. *Front Neurosci.* 2016;10:45.
25. Catafau AM, Bullich S, Seibyl JP, et al. Cerebellar amyloid-beta plaques: how frequent are they, and do they influence ^{18}F-florbetaben SUV ratios? *J Nucl Med.* 2016;57:1740–1745.
26. Blume T, Focke C, Peters F, et al. Microglial response to increasing amyloid load saturates with aging: a longitudinal dual tracer in vivo muPET-study. *J Neuroinflammation.* 2018;15:307.
27. Ulrich JD, Ulland TK, Mahan TE, et al. ApoE facilitates the microglial response to amyloid plaque pathology. *J Exp Med.* 2018;215:1047–1058.
28. Brendel M, Kleinberger G, Probst F, et al. Increase of TREM2 during aging of an Alzheimer's disease mouse model is paralleled by microglial activation and amyloidosis. *Front Aging Neurosci.* 2017;9:8.
29. Foley AM, Ammar ZM, Lee RH, Mitchell CS. Systematic review of the relationship between amyloid-beta levels and measures of transgenic mouse cognitive deficit in Alzheimer's disease. *J Alzheimers Dis.* 2015;44:787–795.
30. Focke C, Blume T, Zott B, et al. Early and longitudinal microglial activation but not amyloid accumulation predict cognitive outcome in PS2APP mice. *J Nucl Med.* 2019;60:548–554.
31. Deleye S, Waldron AM, Verhaeghe J, et al. Evaluation of small-animal PET outcome measures to detect disease modification induced by BACE inhibition in a transgenic mouse model of Alzheimer disease. *J Nucl Med.* 2017;58:1977–1983.
32. Meier SR, Syvanen S, Hultqvist G, et al. Antibody-based in vivo PET imaging detects amyloid-beta reduction in Alzheimer transgenic mice after BACE-1 inhibition. *J Nucl Med.* 2018;59:1885–1891.

Asymmetry of Fibrillar Plaque Burden in Amyloid Mouse Models

Christian Sacher[1], Tanja Blume[1,2], Leonie Beyer[1], Gloria Biechele[1], Julia Sauerbeck[1], Florian Eckenweber[1], Maximilian Deussing[1], Carola Focke[1], Samira Parhizkar[3], Simon Lindner[1], Franz-Josef Gildehaus[1], Barbara von Ungern-Sternberg[1], Karlheinz Baumann[4], Sabina Tahirovic[2], Gernot Kleinberger[3,5,6], Michael Willem[3], Christian Haass[2,3,5], Peter Bartenstein[1], Paul Cumming[7,8], Axel Rominger[1,7], Jochen Herms[2,5,9], and Matthias Brendel[1,5]

[1]Department of Nuclear Medicine, University Hospital of Munich, Ludwig Maximilian University Munich, Munich, Germany; [2]German Center for Neurodegenerative Diseases, Munich, Germany; [3]Biomedical Center, Faculty of Medicine, Ludwig Maximilian University Munich, Munich, Germany; [4]Roche Pharma Research and Early Development, F. Hoffmann-La Roche Ltd., Basel, Switzerland; [5]Munich Cluster for Systems Neurology (SyNergy), Munich, Germany; [6]ISAR Bioscience GmbH, Planegg, Germany; [7]Department of Nuclear Medicine, Inselspital, University Hospital Bern, Bern, Switzerland; [8]School of Psychology and Counselling and IHBI, Queensland University of Technology, Brisbane, Australia; and [9]Center of Neuropathology and Prion Research, University of Munich, Munich, Germany

Asymmetries of amyloid-β (Aβ) burden are well known in Alzheimer disease (AD) but did not receive attention in Aβ mouse models of Alzheimer disease. Therefore, we investigated Aβ asymmetries in Aβ mouse models examined by Aβ small-animal PET and tested if such asymmetries have an association with microglial activation. **Methods:** We analyzed 523 cross-sectional Aβ PET scans of 5 different Aβ mouse models (APP/PS1, PS2APP, APP-SL70, App^{NL-G-F}, and APPswe) together with 136 18-kDa translocator protein (TSPO) PET scans for microglial activation. The asymmetry index (AI) was calculated between tracer uptake in both hemispheres. AIs of Aβ PET were analyzed in correlation with TSPO PET AIs. Extrapolated required sample sizes were compared between analyses of single and combined hemispheres. **Results:** Relevant asymmetries of Aβ deposition were identified in at least 30% of all investigated mice. There was a significant correlation between AIs of Aβ PET and TSPO PET in 4 investigated Aβ mouse models (APP/PS1: $R = 0.593$, $P = 0.001$; PS2APP: $R = 0.485$, $P = 0.019$; APP-SL70: $R = 0.410$, $P = 0.037$; App^{NL-G-F}: $R = 0.385$, $P = 0.002$). Asymmetry was associated with higher variance of tracer uptake in single hemispheres, leading to higher required sample sizes. **Conclusion:** Asymmetry of fibrillar plaque neuropathology occurs frequently in Aβ mouse models and acts as a potential confounder in experimental designs. Concomitant asymmetry of microglial activation indicates a neuroinflammatory component to hemispheric predominance of fibrillary amyloidosis.

Key Words: asymmetry; amyloid; microglia; mouse models

J Nucl Med 2020; 61:1825–1831
DOI: 10.2967/jnumed.120.242750

Alzheimer disease (AD) is the most frequent neurodegenerative disease, with burgeoning incidence rates due to the rising life expectancy in most of the world (*1*). The neuropathology of AD is histologically characterized by the triad of accumulation of amyloid-β (Aβ) peptide as extracellular plaques, aggregation of fibrillary tau protein within neurons, and activation of multiple neuroinflammatory pathways, as mediated by activated microglia expressing high levels of the marker 18-kDa translocator protein (TSPO) (*2*). Animal models that accurately reflect this complex pathology are indispensable for contemporary preclinical research into the molecular mechanisms of AD. In this context, a range of different overexpressing and knock-in Aβ mouse models has been established for molecular imaging with PET. In recent PET studies, increased binding of the Aβ tracer ^{18}F-florbetaben and the TSPO tracer ^{18}F-GE-180 was firmly established by longitudinal in vivo quantification of cerebral amyloidosis and microglial activation in various Aβ mouse models of AD (*3–5*). In humans, an asymmetric spatial distribution of neuropathologic AD hallmarks is frequently discovered by PET studies in vivo (*6–8*). A recent human PET study has already shown that asymmetric spatial distributions of Aβ plaques are positively correlated with ipsilateral neurodegeneration (*8*). However, no study has hitherto systematically investigated the asymmetry in Aβ mouse models of AD. Although a large-scale investigation of this phenomenon by histopathologic investigations would be costly and difficult in terms of standardization, in vivo PET imaging methods should afford the means to readily compare the Aβ plaque burden in both hemispheres of individual animals.

Given this background, our aim was to investigate the occurrence of asymmetric fibrillar Aβ deposition in the well-established Aβ mouse models APP/PS1, PS2APP, APP-SL70, App^{NL-G-F}, and APPswe. Using a large series of historical ^{18}F-florbetaben Aβ PET recordings, we tested for asymmetric Aβ deposition while considering age as a predictive variable. We also estimated sample sizes for detecting asymmetric Aβ and tested the hypothesis that Aβ asymmetry is associated with ipsilateral microglial activation as assessed by ^{18}F-GE-180 TSPO PET.

MARTERIAL AND METHODS

Experimental Design

All experiments were performed in compliance with the German National Guidelines for Animal Protection and with the approval of

Received Jan. 30, 2020; revision accepted Apr. 3, 2020.
For correspondence or reprints contact: Matthias Brendel, Department of Nuclear Medicine, University of Munich, Marchioninistrasse 15, 81377 Munich, Germany.
E-mail: matthias.brendel@med.uni-muenchen.de
Published online May 15, 2020.

the regional animal committee (Regierung Oberbayern) and were overseen by a veterinarian. Animals were housed in a temperature- and humidity-controlled environment with a 12-h light–dark cycle, with free access to food (Sniff) and water. A detailed overview of the investigated mouse cohorts is given in Supplemental Table 1 (supplemental materials are available at http://jnm.snmjournals.org). All PET raw data originated from previous in-house studies (cited below) conducted on the same Inveon small-animal PET scanner under identical acquisition parameters. Of the mice investigated, 87% were female. APP/PS1 and APPswe comprised only female mice, whereas PS2APP, APP-SL70, and $App^{NL\text{-}G\text{-}F}$ included both sexes. All raw data were reprocessed to guarantee optimal agreement of spatial and radioactivity normalization. Either descriptive datasets or control groups of therapy and genotype studies were included. From each investigated mouse, the degree of asymmetry in Aβ PET and TSPO PET was assessed by volume-of-interest–based quantification in both cerebral hemispheres.

Animal Models

APP/PS1 (APPPS1-21). This transgenic mouse model was generated on a C57BL/6J genetic background that coexpresses KM670/671NL mutated amyloid precursor protein (APP) and L166P mutated presenilin (PS) 1 under the control of a neuron-specific Thy1 promoter. Cerebral amyloidosis in this model starts at 6–8 wk of age (*9*). Historical ^{18}F-florbetaben data from 41 scans of APP/PS1 mice imaged at 4 different ages (3, 6, 9, and 12 mo) were reprocessed (*10*). Twenty-seven contemporaneous ^{18}F-GE-180 scans were available.

PS2APP (APPswe/PS2). The transgenic B6.PS2APP (line B6.152H) is homozygous both for human PS2, the N141I mutation, and for the human APP K670N/M671L mutation (*11*). Homozygous B6.PS2APP mice first show plaques in the cerebral cortex and hippocampus at 5–6 mo of age (*12*). Historical ^{18}F-florbetaben data from 147 scans of PS2APP mice imaged at 4 different age ranges (6–8, 9–10, 11–14, and 15–17 mo) were reprocessed (*13,14*). Twenty-three contemporaneous ^{18}F-GE-180 scans from these mice were likewise reprocessed by standard methods.

APP-SL70. The PS1 knock-in line was generated by introducing 2-point mutations in the wild-type (WT) mouse PSEN1, corresponding to the mutations M233T and L235P. The APP751SL mouse overexpresses human APP751 carrying the London (V717I) and Swedish (K670N/M671L) mutations under the control of the Thy1 promoter. Aβ deposits appear as early as 2.5 mo of age in these mice (*15*). Historical ^{18}F-florbetaben data from 208 scans of APP-SL70 mice imaged at 4 different ages (4–6, 7–9, 10–12, and 13–15 mo), deriving from a descriptive observational study (*16*), along with control scans from an as-yet-unpublished therapy study were reprocessed. Twenty-six contemporaneous ^{18}F-GE-180 scans were available in this group.

$App^{NL\text{-}G\text{-}F}$ ($App^{NL\text{-}G\text{-}F/NL\text{-}G\text{-}F}$). The knock-in mouse model $App^{NL\text{-}G\text{-}F}$ carries a mutant *APP* gene encoding the humanized Aβ sequence (G601R, F606Y, and R609H) with 3 pathogenic mutations, namely Swedish (KM595/596NL), Beyreuther/Iberian (I641F), and Arctic (E618G). Homozygotic $App^{NL\text{-}G\text{-}F}$ mice progressively exhibit widespread Aβ accumulation from 2 mo of age (*17,18*). Historical ^{18}F-florbetaben data from 55 scans of homozygotic $App^{NL\text{-}G\text{-}F}$ mice imaged at 4 different ages (2.5, 5.0, 7.5, and 10 mo) were reprocessed (*3*). Fifty-five contemporaneous ^{18}F-GE-180 scans were available in this dataset.

APPswe. Transgenic mice overexpressing human APP with the Swedish double mutation (K670N, M671L) driven by the mouse Thy1.2 promoter were generated as described earlier (*11*). Mice heterozygous for the transgene begin accumulating β-amyloid at approximately 9 mo of age and develop β-amyloid plaques at 12 mo of age, mainly in the cortical mantle. Historical ^{18}F-florbetaben data from 72 scans of APPswe mice imaged at 3 different age ranges (9–12, 13–16, and 17–20 mo) were reanalyzed (*19,20*). Contemporaneous ^{18}F-GE-180 scans were not available for these mice.

C57Bl/6. Historical and unpublished ^{18}F-florbetaben data from 27 scans of C57BL/6 mice (WT) were reprocessed and served as control material (age, 2.5–16 mo).

PET Imaging

PET Data Acquisition, Reconstruction, and Postprocessing. For all PET procedures, radiochemistry, data acquisition, and image preprocessing were conducted according to an established, standardized protocol (*4,21*). In brief, ^{18}F-florbetaben Aβ PET recordings (average dose, 11.4 ± 2.0 MBq) with an emission window of 30–60 min after injection were obtained to measure fibrillar cerebral amyloidosis. ^{18}F-GE-180 TSPO PET recordings (average dose, 11.1 ± 2.0 MBq) with an emission window of 60–90 min after injection were performed for assessment of cerebral TSPO expression. Anesthesia was maintained from just before tracer injection to the end of the imaging time window.

PET Image Analysis. We performed all analyses using PMOD (version 3.5; PMOD technologies). Emission images were normalized to SUV ratio (SUVR) images using previously validated white matter reference regions for transgenic amyloid mouse models (APP/PS1, PS2APP, APP-SL70, and APPswe) (*4,21*). For the knock-in mouse line $App^{NL\text{-}G\text{-}F}$, the mesencephalic periaqueductal gray was used as a reference region, as recently published (*3*). Two bilateral telencephalic volumes of interest (containing cortex and hippocampus) comprising 50 mm^3 each were used for calculation of the forebrain–to–white matter SUVR or the forebrain–to–periaqueductal gray SUVR. For each scan, the hemispheric asymmetry index (AI) was calculated for ^{18}F-florbetaben or ^{18}F-GE-180 scans using the following formula:

$$\text{AI}\ (\%) = 200 \times (\text{L} - \text{R})/(\text{L} + \text{R}).$$

Statistical Analysis

We calculated 95% and 99% confidence intervals (CIs) for ^{18}F-florbetaben AIs in normal C57BL/6 mice. Aβ mouse model ^{18}F-florbetaben scans were judged as asymmetric when they exceeded the 95%CI (moderate asymmetry) or the 99%CI (strong asymmetry) of C57BL/6 mice. Significant ^{18}F-florbetaben |AIs| (absolute magnitude) were correlated with age for each Aβ mouse model to evaluate the age dependency of asymmetric plaque distribution. For each Aβ mouse model, age-independent lateralized plaque distributions were compared by a χ^2 test to test for left or right predominance of Aβ deposition. The frequency of strong asymmetries was calculated in groups of comparable age for Aβ mouse models and correlated with the coefficient of variance for SUVR in the same groups of mice. Pearson coefficients of correlation were calculated for the latter analyses and for correlation analyses between ^{18}F-florbetaben AIs and age, as well as between ^{18}F-florbetaben AIs and ^{18}F-GE-180 AIs. Hypothetic 2-sided *t* tests of independent measures were done to calculate sample sizes for comparisons of SUVR in single hemispheres with SUVR in combined hemispheres using G*Power (version 3.1.9.2). We used a given 5% therapy effect on SUVR at a power (1 − β) of 0.80 and type 1 error with an α value of 0.05. A *P* value of less than 0.05

was considered to be significant for rejection of the null hypothesis. SPSS 25 statistics (IBM Deutschland GmbH) was used for all statistical tests.

RESULTS

Asymmetric Plaque Distribution Is Frequent in Aβ Mouse Models

First, we defined an asymmetry threshold based on PET measurements in WT mice to establish real Aβ asymmetry, without bias in the spatial normalization or by physiologic variability in tracer uptake. The 95%CI of ^{18}F-florbetaben AIs in C57BL/6 mice was −3.6% (right lateralization) to 3.6% (left lateralization) and defined the threshold for moderate Aβ asymmetry. The 99%CI of ^{18}F-florbetaben AIs in C57BL/6 was −4.0% (right lateralization) to 4.5% (left lateralization) and defined the threshold for strong Aβ asymmetry. Using these thresholds, 40% (left, 21%; right, 19%; 95%CI) of all amyloid-accumulating mice showed moderate asymmetry of ^{18}F-florbetaben forebrain uptake and 30% (left, 14%; right, 16%; 99%CI) showed strong asymmetry (Fig. 1). There was no significant hemispheric predominance across the whole cohort of different Aβ mouse models. A detailed overview is provided in Supplemental Table 1.

The highest frequency of moderate Aβ PET asymmetry was observed in PS2APP and *App*$^{NL\text{-}G\text{-}F}$ mice (49% each). Strong Aβ PET asymmetry was most frequently observed in PS2APP and APP/PS1 mice (37% each). The lowest frequency of Aβ PET asymmetry was present in APPswe mice, in which 32% of scans indicated moderate and 24% strong asymmetry. A significant left-hemispheric predominance of Aβ deposition was detected in the PS2APP mice ($\chi^2 = 4.7$; $P = 0.030$), whereas a significant right-hemispheric predominance of Aβ deposition was seen in APPswe mice ($\chi^2 = 15$; $P = 0.0001$). There was no significant association between age and asymmetric Aβ distribution in any Aβ mouse model (Fig. 2). In summary, asymmetry of plaque burden was frequently observed in all studied Aβ mouse models, but with different magnitudes and side predilections.

Asymmetric Plaque Burden Impacts the Sufficient Sample Sizes in Preclinical Trials

Given the observed asymmetries in all Aβ mouse models studied, we hypothesized that measures in single hemispheres (as are

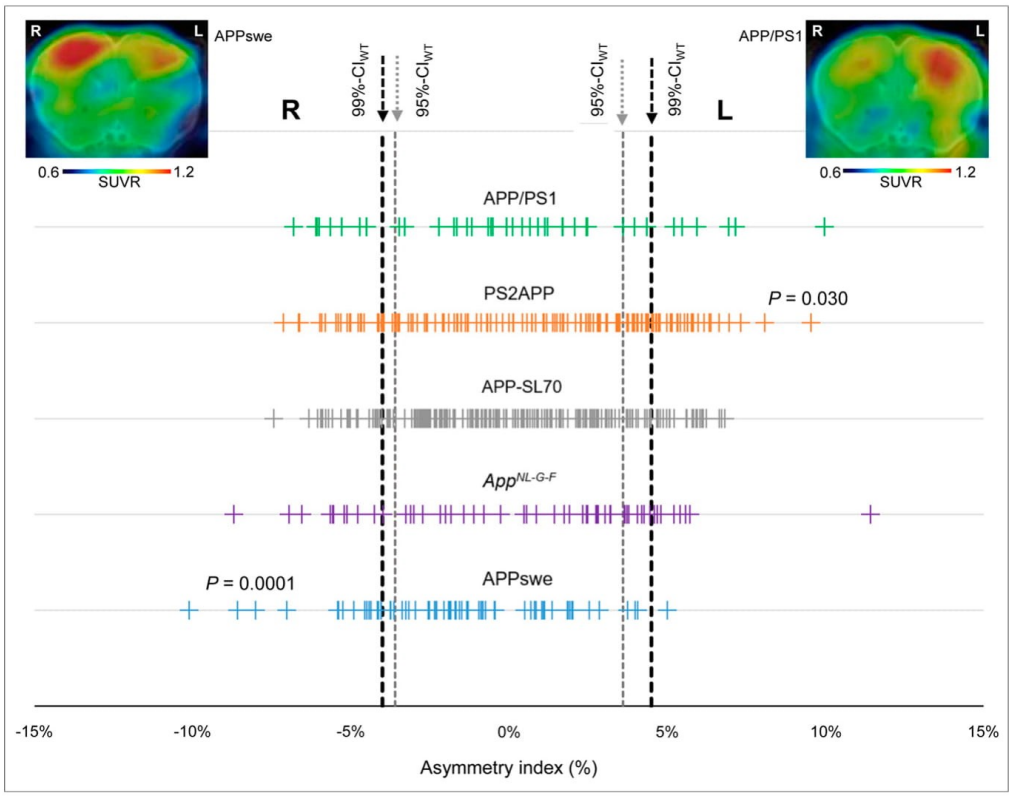

FIGURE 1. Asymmetry of plaque distribution in amyloid mouse models. Forest plot shows AI for total of 523 amyloid PET scans in APP/PS1, PS2APP, APP-SL70, APPswe, and *App*$^{NL\text{-}G\text{-}F}$ mice. Lateralized plaque distributions were compared by χ^2 test to test for left or right predominance in each mouse model. Representative PET SUVR images show exemplary mice with right (APPSwe) and left (APP/PS1) asymmetry.

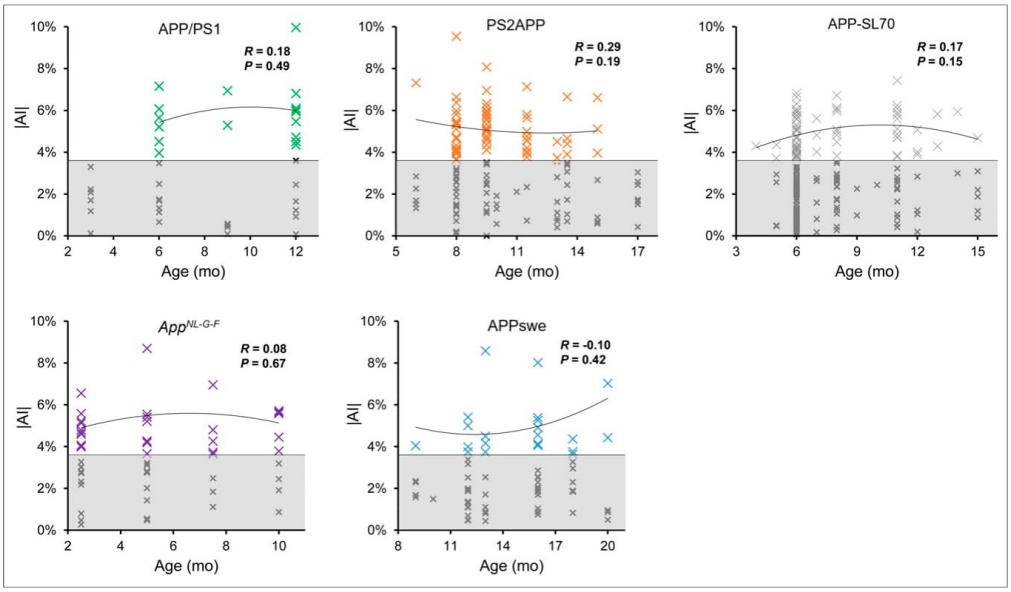

FIGURE 2. Age dependency of asymmetric amyloid deposition. Asymmetry (|AI|) is shown as function of age for APP/PS1, PS2APP, APP-SL70, APPswe, and *App*$^{NL\text{-}G\text{-}F}$ mice. Datapoints with significant asymmetric ^{18}F-florbetaben uptake ($|AI| > 95\%CI_{WT}$; white area) indicate no relevant dependency of asymmetric plaque distribution on age in any mouse models. Values with symmetric distribution (gray area) were excluded from correlation analysis.

typically examined by histologic methods) would suffer from higher variance, subsequently leading to increased required sample sizes in preclinical trials when compared with combined measures of both hemispheres, as are obtained by PET. Coefficient of variance was positively associated with the frequency of plaque burden asymmetry (99%CI) in groups of comparable age in different Aβ mouse models ($R = 0.380$, $P = 0.027$, Fig. 3A). Coefficient of variance by groups of comparable age in the different Aβ mouse models was 4.3% ± 1.2% for separate measures of left and right hemispheres and significantly lower for the combined quantification of both hemispheres (3.9% ± 1.2%; $P = 0.0003$, left vs. both; $P = 0.0007$, right vs. both; paired *t* test). For detection of a 5% therapy effect on SUVR at a power ($1 - \beta$) of 0.80 and type 1 error with an α value of 0.05, calculated sample sizes were 14.1 for separate measures for the left hemisphere, 13.9 for separate measures of the right hemisphere, and 11.9 for combined quantification of both hemispheres ($P = 0.0020$ and 0.0016 for left vs. both and right vs. both, respectively; paired *t* test). Required

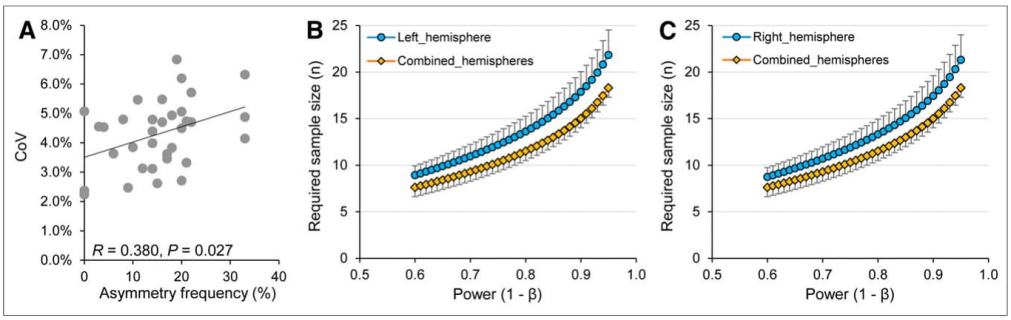

FIGURE 3. Statistical relevance of asymmetric plaque distribution in amyloid mouse models. (A) Association of higher coefficients of variation (CoV) in SUVR with higher frequency of asymmetry in age-related groups of amyloid mouse models (Supplemental Table 1). (B and C) Required sample sizes as function of power in comparison of analyses in single hemispheres and combined hemispheres (given effect of 5%, α = 0.05, hypothetical 2-sided *t* test of independent measures).

sample sizes as a function of power were consistently increased for calculation with left (Fig. 3B) and right (Fig. 3C) hemispheric values when compared with combined quantification of both hemispheres. The average reductions in required sample sizes for combined quantification of both hemispheres were 2.1 ± 0.6 (vs. left) and 1.8 ± 0.5 (vs. right). These results indicate that asymmetry of plaque burden in Aβ mouse models considerably increases required sample sizes when hemispheres are analyzed separately.

Asymmetric Plaque Burden Is Associated with Ipsilateral Glial Activation

Several studies have revealed associations between amyloid deposition and microglial activation in Aβ mouse models (*3,4,16*). However, it has not hitherto been investigated if microglial activation follows any asymmetry of plaque burden or if the microgliosis is globally distributed. Hence, we made use of contemporaneous TSPO PET data for correlation analysis with lateralization to Aβ PET. Significant positive associations between asymmetric Aβ deposition and ipsilateral lateralization of TSPO expression were observed in all 4 Aβ mouse models (Fig. 4). The magnitude of correlation between asymmetric Aβ PET and ipsilateralized TSPO PET uptake was similar among APP/PS1 ($R = 0.593$; $P = 0.001$; $n = 27$; Pearson correlation), PS2APP ($R = 0.485$; $P = 0.019$; $n = 23$; Pearson correlation), APP-SL70 ($R = 0.410$; $P = 0.037$; $n = 26$; Pearson correlation), and $App^{NL\text{-}G\text{-}F}$ ($R = 0.385$; $P = 0.002$; $n = 60$; Pearson correlation) mice. Taken together these results clearly indicate a spatial association between asymmetric distribution of fibrillar Aβ plaques and ipsilateral microglial activation.

DISCUSSION

In contrast to human investigations on asymmetric Aβ distribution in AD (*6,8,22*), only scant evidence is available for the presence of Aβ asymmetry in mouse models (*19,23*). We present the first large-scale preclinical in vivo investigation of fibrillar plaque burden asymmetry by standardized evaluation of PET data. With respect to animal welfare guidelines, in particular reduction of animal numbers in accordance with the 3R principle (replacement, reduction, and refinement), we used scans from various earlier studies, thus avoiding any requirement for additional animal experiments to test our hypotheses.

First, we endeavored to establish a reasonable threshold of lateralized Aβ PET signal to exclude asymmetry findings driven by reasons other than Aβ pathology. To this end, we used Aβ PET data of C57BL/6 WT mice, as they are not known to manifest any Aβ accumulation. Minor asymmetry of florbetaben tracer uptake in WT mice could be attributed to factors such as differences in cerebral blood flow, differing hemispheric volumes, or methodologic issues such as lateralized spillover of bone uptake, imperfect attenuation correction, or bias in spatial normalization. Hence, we used the 95%CI and 99%CI of ^{18}F-florbetaben AIs in WT to discern moderate and strong asymmetry in the groups of Aβ-accumulating mice. By these criteria, 40% of all Aβ-accumulating mice revealed moderate asymmetry, and 30% showed strongly asymmetric Aβ deposition, but without evidence for a general lateralization across all AD models. Nevertheless, 2 of 5 investigated amyloid models revealed significant lateralization of Aβ plaque distribution to Aβ PET. There was a significant left-hemispheric

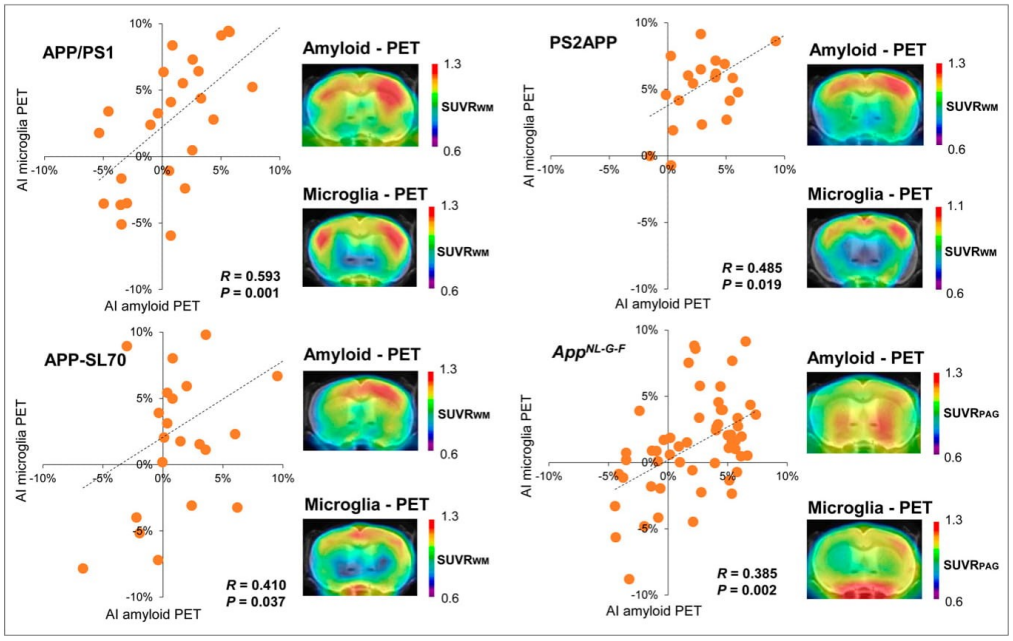

FIGURE 4. Association between lateralized amyloid deposition and microglia activation. Correlations between AIs of amyloid and microglia PET in APP/PS1, PS2APP, APP-SL70, and $App^{NL\text{-}G\text{-}F}$ mice show congruent asymmetry of both biomarkers. PAG = periaqueductal gray; WM = white matter.

predominance of Aβ deposition in PS2APP mice, but a significant right-hemispheric predominance in APPswe mice. Although molecular explanations and causal mechanisms giving rise to this phenomenon are presently unknown, we contend that this is a real phenomenon requiring special consideration when comparing data from different Aβ mouse models of AD. For example, a comparison of exclusively right-hemisphere readouts, as might be obtained by histologic analysis, between APPswe and PS2APP could cause false-negative findings, and likewise for the left hemisphere. The highest frequency of asymmetry was observed in Aβ models with a presenilin mutation (PS2APP and APP/PS1), indicating that involvement of this gene might increase the probability of asymmetric plaque burden. Variable expression of APP messenger RNA across different PS2APP mice is already postulated to be a key determinant of variance in individual Aβ deposition (*12*); therefore, we speculate that this phenomenon could likewise hold true for differences between hemispheres.

By making sample-size estimations, we established that the observed asymmetries of fibrillar plaque burden are potentially relevant to the design of preclinical trials. Importantly, the calculated sample sizes sufficient to detect relevant therapeutic effects, which are comparable to those of earlier drug trials in these Aβ mouse models (*13,20*), were significantly higher when only single hemispheres were analyzed, as opposed to combined measurement of both hemispheres. As Aβ PET and histology markers for fibrillar Aβ were strongly intercorrelated in previous studies (*10,19,24*), we assume that asymmetry effects on required sample sizes should also hold true for stand-alone histologic or biochemical analyses. This conjecture remains to be demonstrated, since usual practice is to process 1 hemisphere for histology and 1 for biochemistry. Aβ PET findings at the terminal time-point could help to identify mice with asymmetric plaque burden, which would allow consecutive adjustment of measures by different modalities in separate hemispheres.

Next, we investigated whether asymmetric Aβ distributions occur in an age-dependent manner. Our cross-sectional analysis of historical PET data did not indicate any significant association of AI with age among the 5 Aβ mouse models. This finding is consistent with our earlier longitudinal ^{18}F-florbetaben PET findings in APPswe, were we incidentally noticed that some animals showed consistently right-sided plaque asymmetry between 13 and 20 mo of age. More precisely, the magnitude of asymmetry in SUVR increased with age, but with no temporal dependence of the AI per se (*19*). In conclusion, Aβ asymmetries, when present, are established at the onset of plaque deposition.

We suppose that there are hitherto few reports on asymmetric plaque burden in Aβ mouse models because of the logistic difficulty of conducting onerous histologic analysis of both hemispheres for sufficient numbers of animals. We performed a metaanalysis of the most recent 56 papers from journals with an impact factor of more than 4 published in the interval 2016–2019 with the key words "amyloid, mouse, model, AD." Of these papers, 38% (21/56) provided detailed information about use of different hemispheres for histology and biochemistry; 81% among those (17/21) assigned a specific hemisphere to a given modality, whereas only 19% (4/21) performed randomization of hemispheres to different modalities. Most of the remaining 35 papers likewise split hemispheres to different modalities, but without detailed information about the selection process. Immunohistochemistry with Aβ antibodies such as 6E10 was most frequently used to assess fibrillar plaques in vitro, whereas other studies used histologic staining with methoxy-X04 or thioflavin S (*14,25*). These studies generally reported immunohistochemical and histologic findings for Aβ quantification from a few representative brain slices of a single hemisphere, whereas the other hemisphere was typically reserved for biochemical assays such as enzyme-linked immunosorbent assay or Western blotting, which are not compatible with tissue fixation. Therefore, evaluation of intraanimal asymmetry in vitro was not feasible because of allocation of the hemispheres for different kinds of analyses. In summary, potential asymmetries of fibrillar plaque burden have been only sparsely considered in published papers during recent years.

Contrary to the case in vitro, Aβ PET allows convenient quantification of amyloid pathology in both whole hemispheres, with the caveat that the PET method has inherent limitations in spatial resolution (*26,27*). Therefore, PET quantification of small brain areas can be challenging, although asymmetry assessment of Aβ plaque burden in large forebrain regions is a rather robust measure. Thus, conducting noninvasive PET examination before assignment of hemispheres to different terminal biochemical or histologic experiments could help to identify and adjust for relevant asymmetries of plaque burden. This possibility should encourage the combined use of PET together with immunohistochemistry and biochemistry readouts.

Another focus of our study was to investigate the relationship between lateralized Aβ deposition and microglial activation. Previous studies by our laboratory have already shown close correlations between fibrillar amyloidosis and TSPO expression in APP/PS1, PS2APP, APP-SL70, and $App^{NL\text{-}G\text{-}F}$ mice (*3,4,10,16*). Although we acknowledge that our findings were anticipated from these earlier findings, we now show for the first time that microglial activation occurs concomitantly in the hemisphere ipsilateral to the predominant fibrillar amyloidosis. This association further strengthens the hypothesis that initial fibrillar Aβ accumulation triggers neuroinflammation mediated by activated microglia (*28*). Another recently published study has also demonstrated a link between amyloidosis and neuroinflammation based on comparative profiling of cortical gene expression in AD patients and an Aβ mouse model (*29*). Comparisons of gene expression between hemispheres of mice with asymmetric amyloidosis could give new insights into the molecular pathways and causal mechanisms underlying asymmetry in AD. PET screening could guide the selection for detailed study of mice with strong asymmetries.

CONCLUSION

Nearly a third of Aβ mice show distinct left or right asymmetry in the deposition of cerebral amyloid. This phenomenon is neglected in most current studies on Aβ mice and calls for consideration in the planning and design of preclinical trials, especially when single hemispheres are investigated by methods ex vivo. The lack of age dependency on asymmetric Aβ distribution implies that genetic factors underlie the development of lateralized amyloidosis in AD model mice. There is a clear association between asymmetries of glial activation and fibrillar amyloidosis in all Aβ mouse models investigated in this study, further strengthening the hypothesis that neuroinflammatory response to fibrillar Aβ contributes to the development of pathology in these mice.

DISCLOSURE

Christian Haass collaborates with Denali Therapeutics, participated on 1 advisory board meeting of Biogen, and received a speaker honorarium from Novartis and Roche. Christian Haass is

chief advisor of ISAR Bioscience. Peter Bartenstein, Axel Rominger, and Matthias Brendel received speaking honoraria from Life Molecular Imaging and GE Healthcare. Matthias Brendel is an advisor of Life Molecular Imaging. Christian Haass is supported by the Koselleck Project HA1737/16-1 of the DFG, the Helmholtz-Gemeinschaft (Zukunftsthema "Immunology and Inflammation"(ZT-0027)), and the Cure Alzheimer's fund. This work was supported by the Deutsche Forschungsgemeinschaft (Matthias Brendel and Axel Rominger BR4580/1-1 and RO5194/1-1). The APPPS1 colony was established from a breeding pair kindly provided by Mathias Jucker (Hertie-Institute for Clinical Brain Research, University of Tübingen, and DZNE-Tübingen). APPswe, PS2APP, and APP-SL70 mice were provided by Hoffmann-La Roche. APPNL-G-F mice were provided by RIKEN BRC through the National Bio-Resource Project of the MEXT, Japan. GE Healthcare made GE-180 cassettes available through an early-access model. No other potential conflict of interest relevant to this article was reported.

KEY POINTS

QUESTION: Do amyloid mouse models have asymmetric plaque distribution and asymmetric neuroinflammation?

PERTINENT FINDINGS: Asymmetry in these amyloid mouse models is frequent and statistically relevant for planning of observational and interventional trials in these mice. Moreover, asymmetries of fibrillar plaque burden and glial activation are positively correlated.

IMPLICATIONS FOR PATIENT CARE: Lateralized distribution of fibrillar plaques is insufficiently considered in experimental studies with amyloid mouse models and a potential confounder in preclinical phases of drug development.

REFERENCES

1. Ziegler-Graham K, Brookmeyer R, Johnson E, Arrighi HM. Worldwide variation in the doubling time of Alzheimer's disease incidence rates. *Alzheimers Dement.* 2008;4:316–323.
2. Heneka MT, Carson MJ, El Khoury J, et al. Neuroinflammation in Alzheimer's disease. *Lancet Neurol.* 2015;14:388–405.
3. Sacher C, Blume T, Beyer L, et al. Longitudinal PET monitoring of amyloidosis and microglial activation in a second-generation amyloid-beta mouse model. *J Nucl Med.* 2019;60:1787–1793.
4. Brendel M, Probst F, Jaworska A, et al. Glial activation and glucose metabolism in a transgenic amyloid mouse model: a triple-tracer PET study. *J Nucl Med.* 2016;57:954–960.
5. Sasaguri H, Nilsson P, Hashimoto S, et al. APP mouse models for Alzheimer's disease preclinical studies. *EMBO J.* 2017;36:2473–2487.
6. Ossenkoppele R, Schonhaut DR, Scholl M, et al. Tau PET patterns mirror clinical and neuroanatomical variability in Alzheimer's disease. *Brain.* 2016;139:1551–1567.
7. Tetzloff KA, Graff-Radford J, Martin PR, et al. Regional distribution, asymmetry, and clinical correlates of tau uptake on [^{18}F]AV-1451 PET in atypical Alzheimer's disease. *J Alzheimers Dis.* 2018;62:1713–1724.
8. Frings L, Hellwig S, Spehl TS, et al. Asymmetries of amyloid-beta burden and neuronal dysfunction are positively correlated in Alzheimer's disease. *Brain.* 2015;138:3089–3099.
9. Radde R, Bolmont T, Kaeser SA, et al. Abeta42-driven cerebral amyloidosis in transgenic mice reveals early and robust pathology. *EMBO Rep.* 2006;7:940–946.
10. Parhizkar S, Arzberger T, Brendel M, et al. Loss of TREM2 function increases amyloid seeding but reduces plaque-associated ApoE. *Nat Neurosci.* 2019;22:191–204.
11. Richards JG, Higgins GA, Ouagazzal AM, et al. PS2APP transgenic mice, coexpressing hPS2mut and hAPPswe, show age-related cognitive deficits associated with discrete brain amyloid deposition and inflammation. *J Neurosci.* 2003;23:8989–9003.
12. Ozmen L, Albientz A, Czech C, Jacobsen H. Expression of transgenic APP mRNA is the key determinant for beta-amyloid deposition in PS2APP transgenic mice. *Neurodegener Dis.* 2009;6:29–36.
13. Brendel M, Jaworska A, Overhoff F, et al. Efficacy of chronic BACE1 inhibition in PS2APP mice depends on the regional Abeta deposition rate and plaque burden at treatment initiation. *Theranostics.* 2018;8:4957–4968.
14. Brendel M, Kleinberger G, Probst F, et al. Increase of TREM2 during aging of an Alzheimer's disease mouse model is paralleled by microglial activation and amyloidosis. *Front Aging Neurosci.* 2017;9:8.
15. Blanchard V, Moussaoui S, Czech C, et al. Time sequence of maturation of dystrophic neurites associated with Abeta deposits in APP/PS1 transgenic mice. *Exp Neurol.* 2003;184:247–263.
16. Blume T, Focke C, Peters F, et al. Microglial response to increasing amyloid load saturates with aging: a longitudinal dual tracer in vivo muPET-study. *J Neuroinflammation.* 2018;15:307.
17. Masuda A, Kobayashi Y, Kogo N, Saito T, Saido TC, Itohara S. Cognitive deficits in single App knock-in mouse models. *Neurobiol Learn Mem.* 2016;135:73–82.
18. Saito T, Matsuba Y, Mihira N, et al. Single App knock-in mouse models of Alzheimer's disease. *Nat Neurosci.* 2014;17:661–663.
19. Rominger A, Brendel M, Burgold S, et al. Longitudinal assessment of cerebral beta-amyloid deposition in mice overexpressing Swedish mutant beta-amyloid precursor protein using ^{18}F-florbetaben PET. *J Nucl Med.* 2013;54:1127–1134.
20. Brendel M, Jaworska A, Herms J, et al. Amyloid-PET predicts inhibition of de novo plaque formation upon chronic gamma-secretase modulator treatment. *Mol Psychiatry.* 2015;20:1179–1187.
21. Overhoff F, Brendel M, Jaworska A, et al. Automated spatial brain normalization and hindbrain white matter reference tissue give improved [(18)F]-florbetaben PET quantitation in Alzheimer's model mice. *Front Neurosci.* 2016;10:45.
22. Raji CA, Becker JT, Tsopelas ND, et al. Characterizing regional correlation, laterality and symmetry of amyloid deposition in mild cognitive impairment and Alzheimer's disease with Pittsburgh compound B. *J Neurosci Methods.* 2008;172:277–282.
23. Manook A, Yousefi BH, Willuweit A, et al. Small-animal PET imaging of amyloid-beta plaques with [^{11}C]PiB and its multi-modal validation in an APP/PS1 mouse model of Alzheimer's disease. *PLoS One.* 2012;7:e31310.
24. Brendel M, Jaworska A, Griessinger E, et al. Cross-sectional comparison of small animal [^{18}F]-florbetaben amyloid-PET between transgenic AD mouse models. *PLoS One.* 2015;10:e0116678.
25. Cho SM, Lee S, Yang SH, et al. Age-dependent inverse correlations in CSF and plasma amyloid-beta(1-42) concentrations prior to amyloid plaque deposition in the brain of 3xTg-AD mice. *Sci Rep.* 2016;6:20185.
26. Visser EP, Disselhorst JA, Brom M, et al. Spatial resolution and sensitivity of the Inveon small-animal PET scanner. *J Nucl Med.* 2009;50:139–147.
27. Huisman MC, Reder S, Weber AW, Ziegler SI, Schwaiger M. Performance evaluation of the Philips MOSAIC small animal PET scanner. *Eur J Nucl Med Mol Imaging.* 2007;34:532–540.
28. Sebastian Monasor L, Müller SA, Colombo AV, et al. Fibrillar Aβ triggers microglial proteome alterations and dysfunction in Alzheimer mouse models. *Elife.* 2020;9:e54083.
29. Castillo E, Leon J, Mazzei G, et al. Comparative profiling of cortical gene expression in Alzheimer's disease patients and mouse models demonstrates a link between amyloidosis and neuroinflammation. *Sci Rep.* 2017;7:17762.